NASA TECHNICAL MEMORANDUM

NASA TM X-64681

APOLLO 15 CONTAMINATION PHOTOGRAPHY

R. J. Naumann
Space Sciences Laboratory

July 5, 1972

NASA

George C. Marshall Space Flight Center
Marshall Space Flight Center, Alabama

MSFC - Form 3190 (Rev June 1971)

TECHNICAL REPORT STANDARD TITLE PAGE

1 REPORT NO.	2 GOVERNMENT ACCESSION NO.	3 RECIPIENT'S CATALOG NO
NASA TM X-64681		

4 TITLE AND SUBTITLE	5 REPORT DATE
Apollo 15 Contamination Photography	July 5, 1972
	6 PERFORMING ORGANIZATION CODE

7 AUTHOR(S)	8 PERFORMING ORGANIZATION REPORT #
R. J. Naumann	

9 PERFORMING ORGANIZATION NAME AND ADDRESS	10 WORK UNIT NO
George C. Marshall Space Flight Center Marshall Space Flight Center, Alabama 35812	11 CONTRACT OR GRANT NO.
	13 TYPE OF REPORT & PERIOD COVERED
12 SPONSORING AGENCY NAME AND ADDRESS	Technical Memorandum
National Aeronautics and Space Administration Washington, D. C. 20546	14 SPONSORING AGENCY CODE

15 SUPPLEMENTARY NOTES

Prepared by Space Sciences Laboratory,
Science and Engineering

16. ABSTRACT

The problem of optical contamination in the form of particulates in the vicinity of a spacecraft has been a source of concern for any astronomical experiment that must be performed in sunlight. This concern prompted a photographic photometric experiment on Apollo 15 to measure the brightness of the residual contamination cloud as well as the cloud produced by dumping waste water overboard.

An upper limit of $10^{-12.3}$ $B_\odot$ ($B_\odot$ designates the brightness of the solar disc) was placed on the residual cloud at a 90-deg sun angle, which is comparable to the zodiacal light. The brightness of the cloud produced by the waste dump was estimated to be $10^{-9.2}$ $B_\odot$. It was observed to decrease rapidly to $10^{-11.6}$ $B_\odot$ in minutes, then fluctuate in brightness for at least 25 minutes as additional material left the spacecraft.

The cloud was observed to consist of individually resolved particle tracks estimated to be particles ranging from millimeters to centimeters in diameter in addition to a background of unresolved particles with an average diameter of 10.5 microns. Most of the tracks proceeded in straight-line paths from the dump nozzle. Several tracks violated this direction, apparently having been scattered by collisions. A few tracks appeared to have definite curvatures, which are believed to be caused by charged particle interactions.

17 KEY WORDS	18 DISTRIBUTION STATEMENT
	Unclassified - unlimited

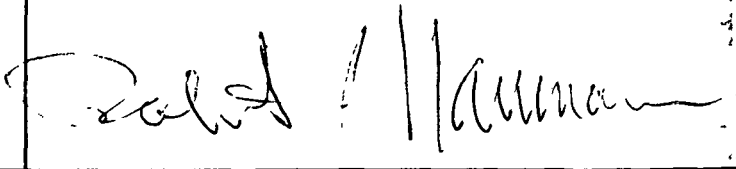

19 SECURITY CLASSIF. (of this report)	20 SECURITY CLASSIF. (of this page)	21 NO. OF PAGES	22 PRICE
Unclassified	Unclassified	62	$3.00

MSFC - Form 3292 (May 1969)

TABLE OF CONTENTS

LIST OF ILLUSTRATIONS

LIST OF ILLUSTRATIONS (Concluded)

LIST OF TABLES

ACKNOWLEDGEMENT

The author wishes to acknowledge the efforts of the personnel at Manned Spacecraft Center and at Marshall Space Flight Center who were involved in this experiment. In particular, he would like to thank Charles Glancy for his untiring support in getting this experiment into the Apollo 15 Mission Flight Plan, Astronauts David Scott and Al Worden for taking the photographs and recording their observations and for their comments and assistance in the analysis, the MSC Photographic Lab for the photographic support, Wally Moore and Bob Gooding for their help in performing the densitometry, and Miss Eva Gatewood for computational support.

APOLLO 15 CONTAMINATION PHOTOGRAPHY

INTRODUCTION

The fact that spacecraft produce their own environment which may interfere with their intended mission was first recognized when John Glenn observed the "fireflies" surrounding his Mercury capsule. Similar observations have been made on all subsequent manned spacecraft, particularly when liquids are dumped overboard, forming ice crystals which act as scattering centers. The amount of light scattered from such particles is significant; for example, the forward scattering just from edge diffraction of sunlight on a 100-micron sphere at a distance of 13 km is equivalent to a third magnitude star. A cloud of such particles will scatter sufficient light to prevent most astronomical experiments from being performed from spacecraft on the sunlight portion of the orbit.

The obvious remedy for this problem was either to refrain from dumping liquids or to time-line the mission such that scheduled dumps would have adequate time to dissipate before astronomical observations were begun. However, there was still a concern that the minimum background from nucleation of H_2O vapor from the escape of cabin gasses, dust particles or paint flecks from spacecraft surface, or other sources of particulates could still be sufficient to produce an intolerable scattered-light background. The evidence for this concern comes primarily from the astronauts' inability to see faint stars in the daytime. Analyses by Newkirk [1] and by Kovar, Kovar, and Bonner [2], assuming some fraction of escaping cabin gasses nucleate into ice crystals with sizes of the order of microns, indicate that the scattered-light background associated with Gemini and Apollo will be several orders of magnitude higher than the solar corona and the zodiacal light. These arguments were refuted by Buffalano and Grobman [3] on the grounds that the maximum size particles that could be produced by such a nucleation process were of the order of 0.01 micron, which would produce negligible scattering. Laboratory tests to determine the size distribution of such particles have been inconclusive. The problem has been avoided on previous dim-light photography experiments performed on Gemini and Apollo missions by photographing only when the spacecraft is in

shadow. However, experiments to observe the sun or the solar corona, such as ATM, cannot avoid the problem in this manner. In fact, the future role of manned space flight in astronomical missions depends on whether manned space vehicles can be designed to keep the optical environment produced by the spacecraft low to avoid interference with the measurements. To date this has not been demonstrated.

The Apollo 15 Contamination Photography Experiment was proposed to investigate the nature of the contamination cloud associated with the Apollo spacecraft. The objective is twofold: (1) to measure the intensity of the contamination cloud associated with the spacecraft in a clean configuration (just prior to a liquid dump with thrusters inhibited) and (2) to evaluate the impact of liquid dumping on seeing conditions.

The clean configuration represents the minimum irreducible contamination environment associated with the Apollo spacecraft. The crucial question is whether the material emanating from the spacecraft is restricted in size such that the scattering is insignificant, or whether there is actually a source of larger material as postulated by Kovar, et al. The first objective was designed to answer this question.

It is known that dumping liquid will produce a large contamination cloud of ice crystals. Such clouds have been observed from ground-based telescopes [4], and certain data such as growth and diffusion rates and integrated brightness have been obtained. Analysis of these data has yielded order of magnitude estimates of particle size and velocity. The second objective was designed to obtain more definitive data on the seeing conditions imposed by this cloud to obtain the decay rate or clearing time for this cloud and to obtain information on the cloud dynamics from the trajectories of individual particles.

DESCRIPTION OF THE EXPERIMENT

The photographs were taken with the 16-mm Data Acquisition Camera (DAC) using an 18-mm f/0.9 lens (Fig. 1). It was intended to use Type 2485 VHBW film; however, film difficulties necessitated substitution of Type SO164 BW film. The camera was mounted in a bracket in window No. 4 with its optical axis perpendicular to the spacecraft X axis. A mirror mounted at 45 deg to the camera axis redirected the optical axis along the X axis. A dark hood over the entire assembly prevented internal light from entering the camera.

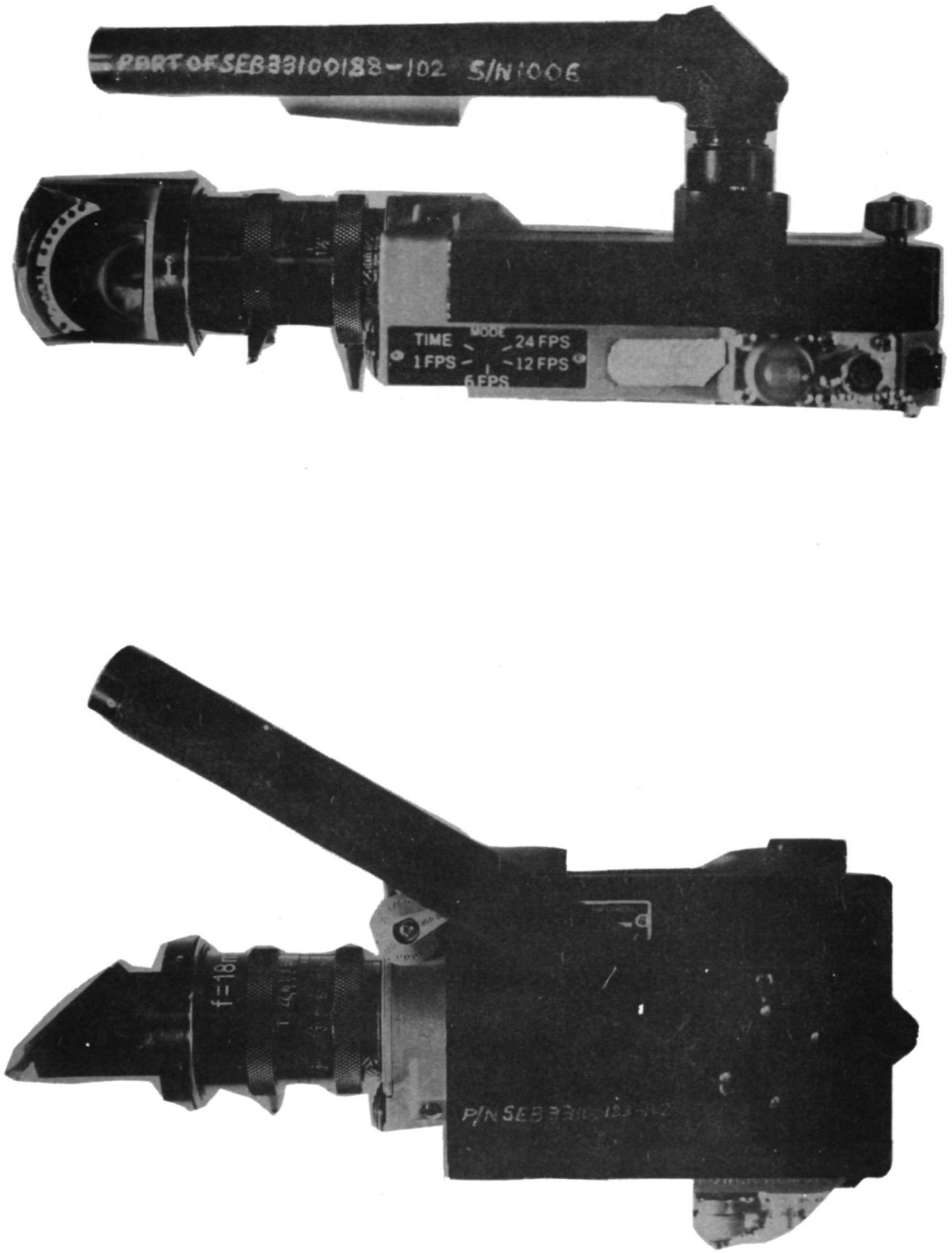

Figure 1. Top and side view of the 16-mm Data Acquisition Camera (DAC) of the type used on Apollo 15. (The 45-deg mirror is attached to the lens, and the boresite telescope is mounted to the side.)

The photographic sequences were taken with the lens at f/0.9 and focused at infinity. The spacecraft was oriented to a predetermined attitude to prevent sunlight, earthlight, and moonlight from being incident on the window. The rates were damped to less than 0.2 deg/sec in all axes. The attitude control system was then placed in "free" mode to prevent thrusters from firing during the photographic sequence.

A sequence consisted of four exposures with times of 1, 20, 60, and 100 sec. These times were chosen to bracket the highest and lowest estimates of the cloud brightness for 2485 film. However, the SO164 film is approximately two orders of magnitude less sensitive than the 2485 film; therefore, the lowest estimates would not be expected to produce detectable fog.

Three sequences were requested: (1) just prior to liquid dumps in a clean configuration, (2) just after completion of the H_2O and urine dumps, and (3) beginning 25 minutes after the dump. Astronaut Scott inserted an extra three frames between the second and third requested sequence, giving a total of four actual sequences.

The photographs were to be taken during the scheduled time for midcourse correction No. 6 if it were not required, which was the case. This time was GET 272:00:00. At the time, the spacecraft was almost halfway between earth and moon. The spacecraft X axis (longitudinal axis, nose positive) was oriented at RA 13 hr 55 min 32 sec, declination - 27° 21' 08". The Z axis was oriented at RA 14 hr 16 min 36 sec, declination 62° 32' 55". The coordinate system used is shown in Figure 2. The location of the earth, sun, and moon as a function of time is given in Figure 3. The position of the earth, moon, and sun is shown on a Θ, ϕ chart in Figure 4, along with the shadow regions for the window. It is seen that the earth and sun are well shadowed by the spacecraft. The moon is incident on the window opening but is almost parallel to the window itself which is inclined at approximately 30 deg to the X axis. The right ascension and declination of the X axis along with the orientation of the Z axis relative to the north celestial pole is shown in Figure 5.

The photographic sequence is shown in Figures 6 through 9 with the exposure time and time relative to dump. Several things should be remembered when viewing the photographs: (1) the prints were made from second generation negatives; therefore, the prints appear as negatives; (2) since the camera photographed through a mirror, right-left parity is reversed. However, the negatives were printed upside down to correct this reversal. Therefore, the orientation in the prints is the same as would be seen by the

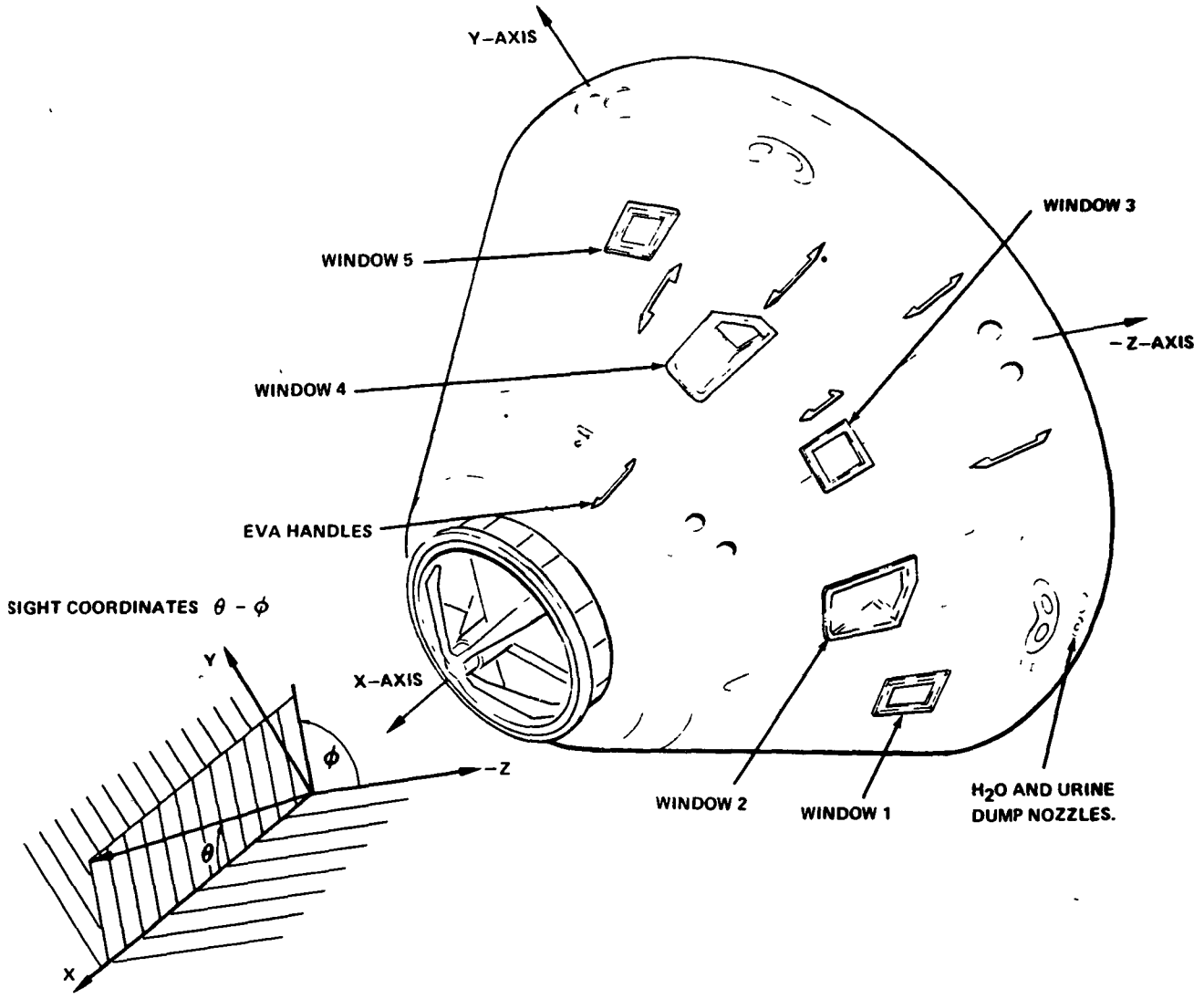

Figure 2. Geometry of the Apollo CSM and of the coordinate system used in this study.

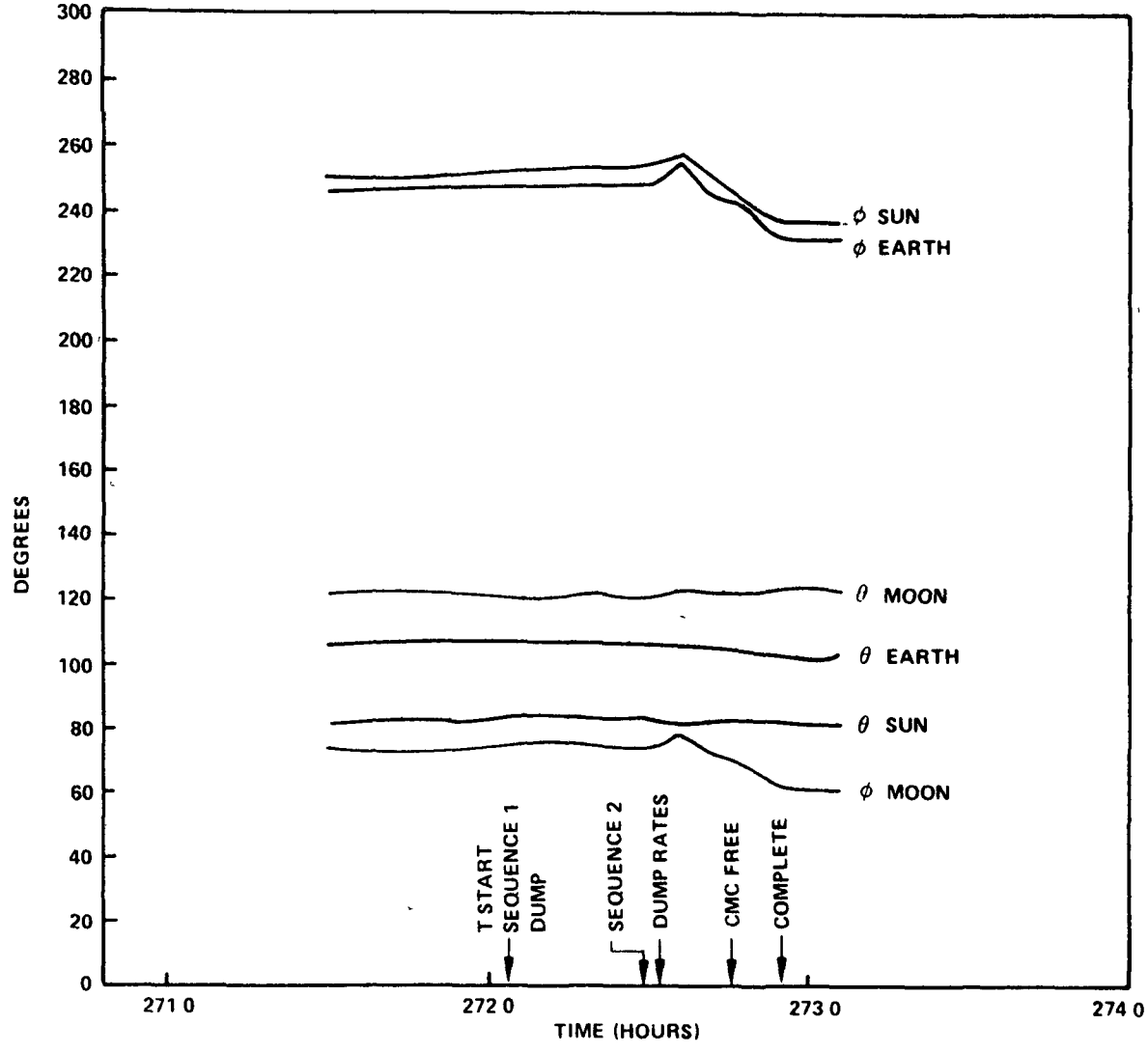

Figure 3. Position of the sun, earth, and moon relative to the spacecraft as a function of time.

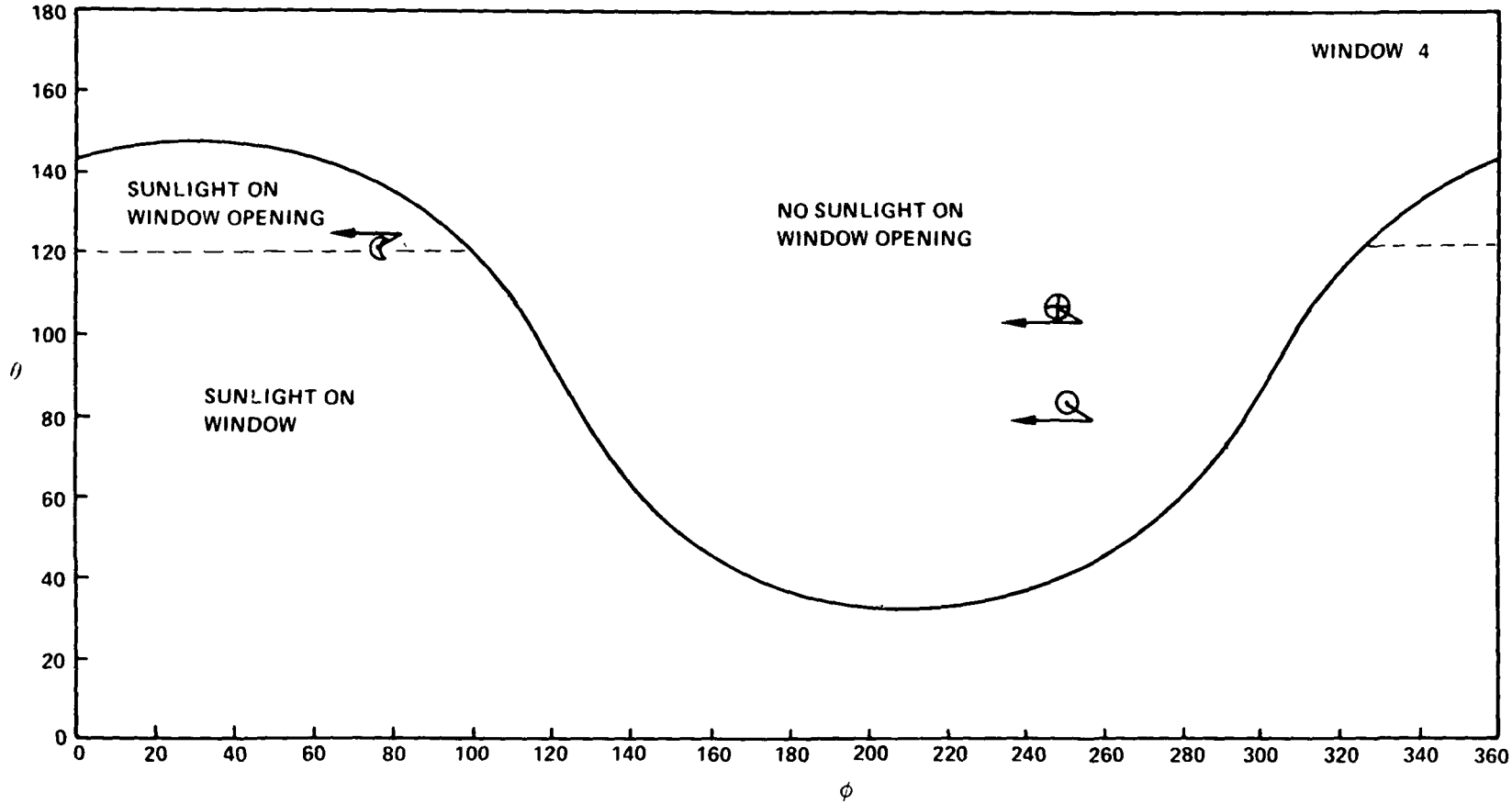

Figure 4. Earth, moon, and sun positions relative to the shadow regions for window 4.

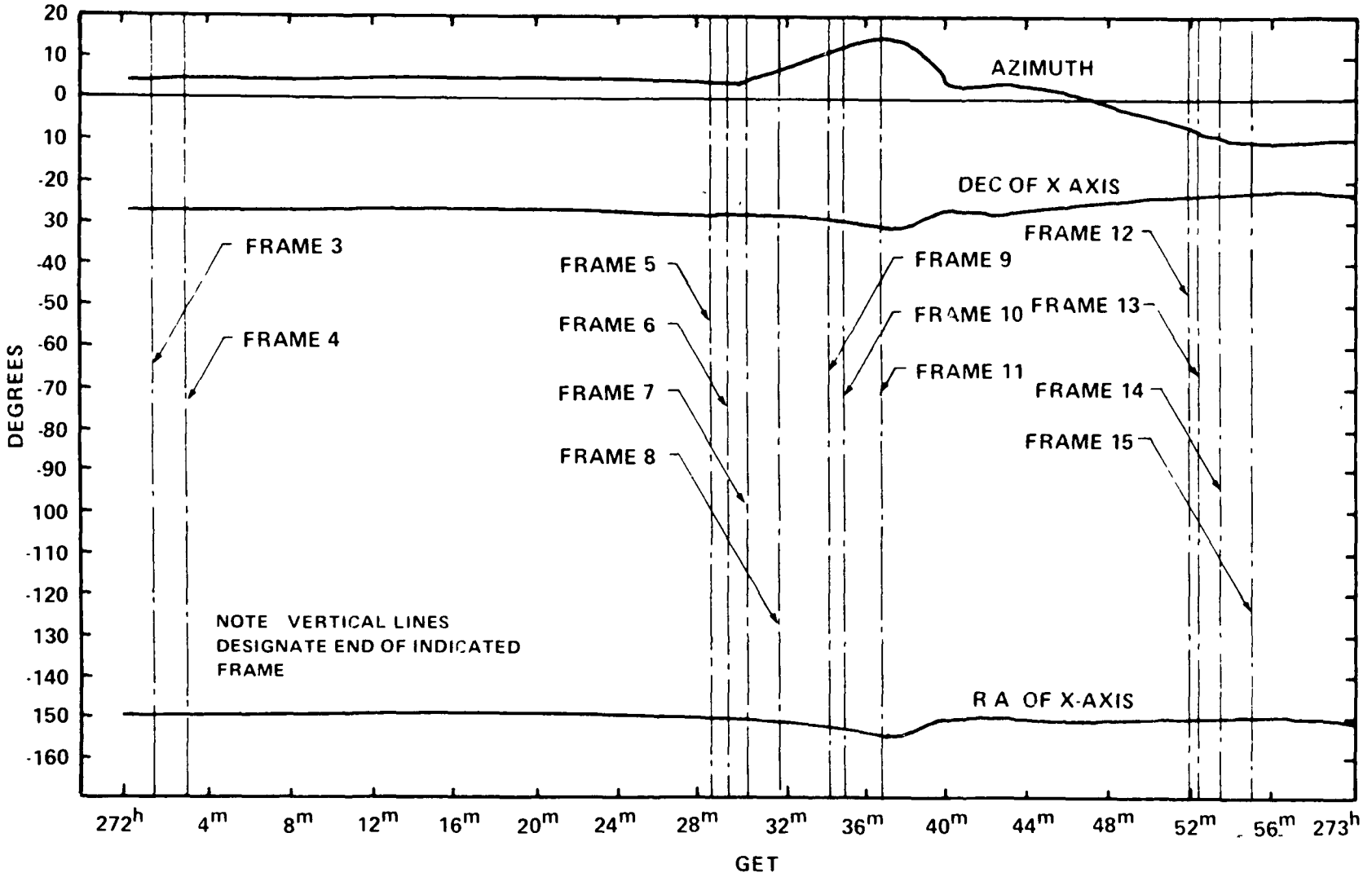

Figure 5. Right ascension and declination of the x axis and the azimuth angle of the z axis as a function of time during the photographic sequence.

BEFORE DUMP

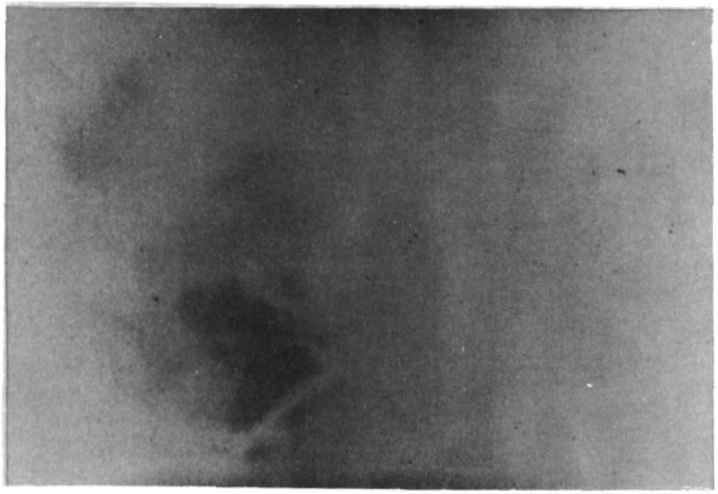

60 SECONDS

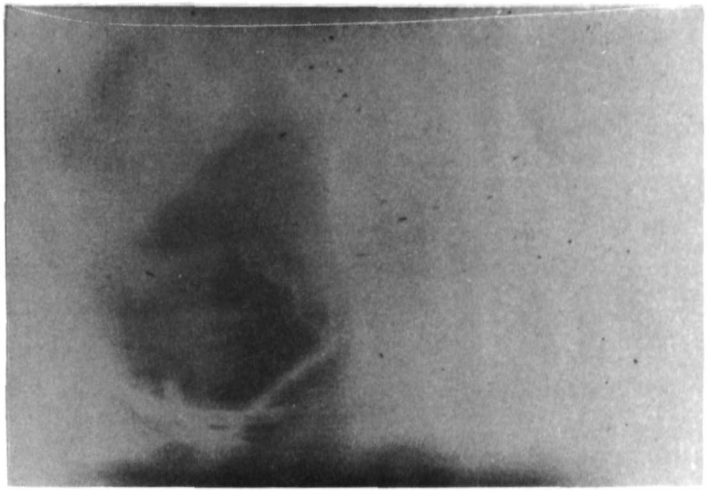

100 SECONDS

Figure 6. Frames 3 and 4 of the photographic sequence.

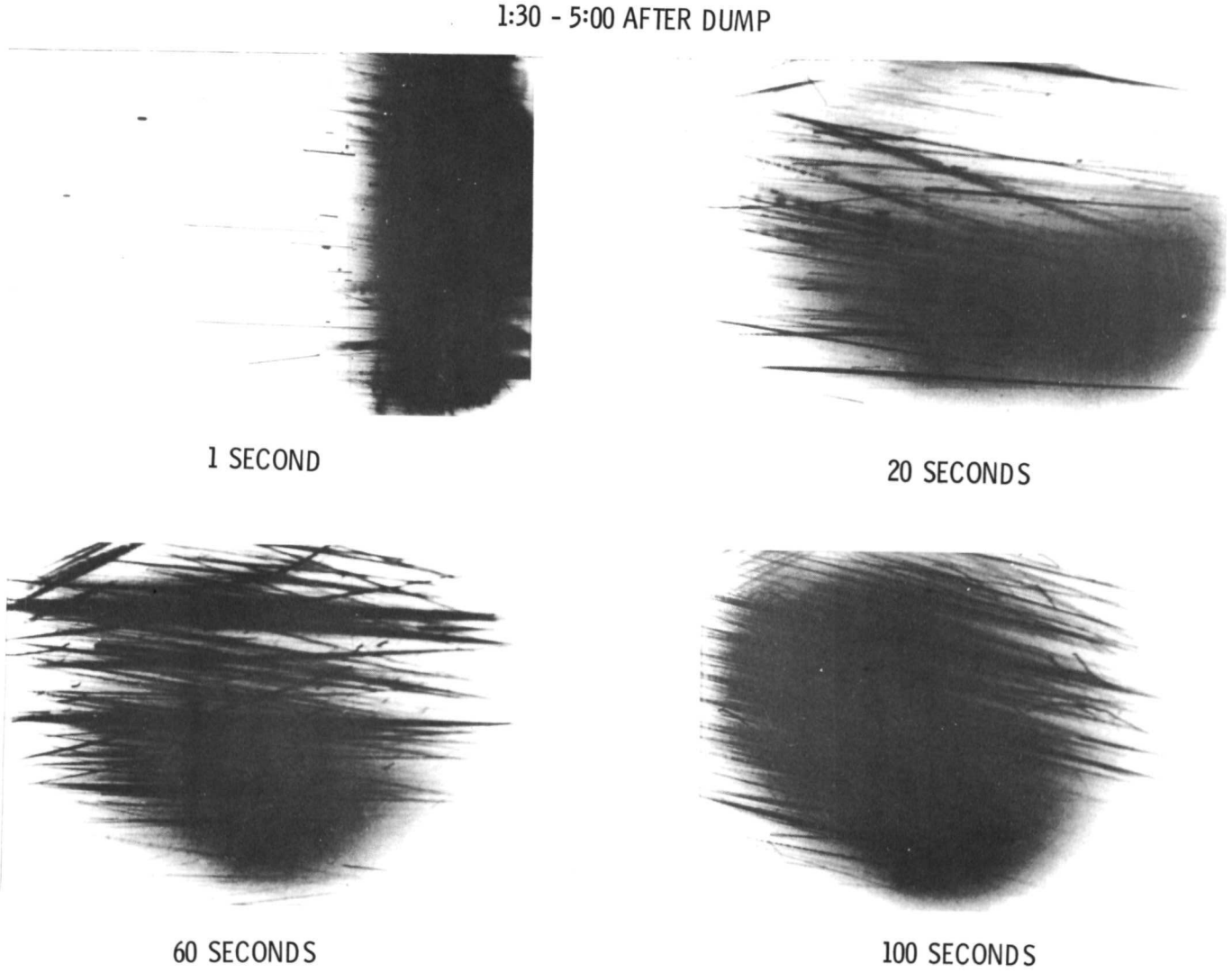

Figure 7. The second photographic sequence for frames 5 through 8.

8:00 - 10:00 AFTER DUMP

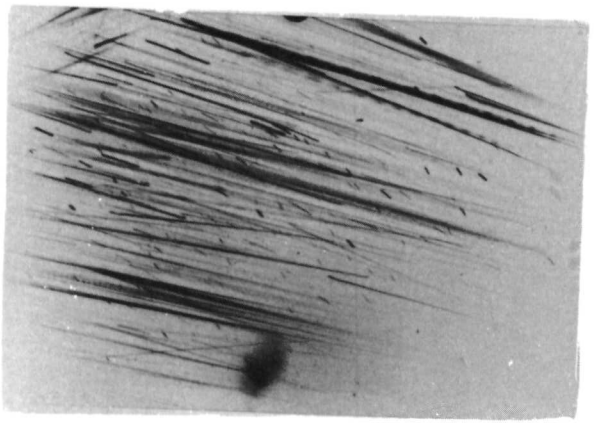

20 SECONDS

60 SECONDS

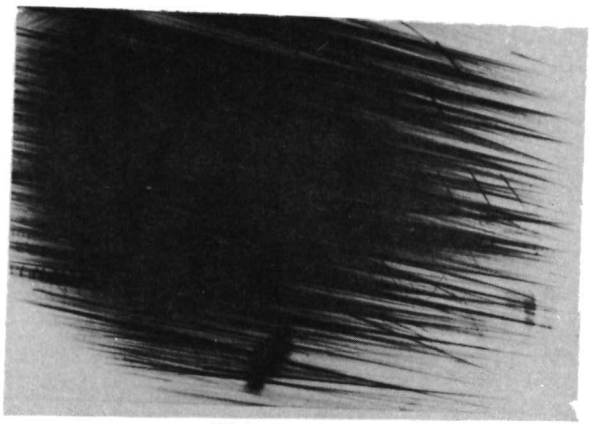

100 SECONDS

Figure 8. Third photographic sequence (frames 9, 10, and 11).

25 - 28 MINUTES AFTER DUMP

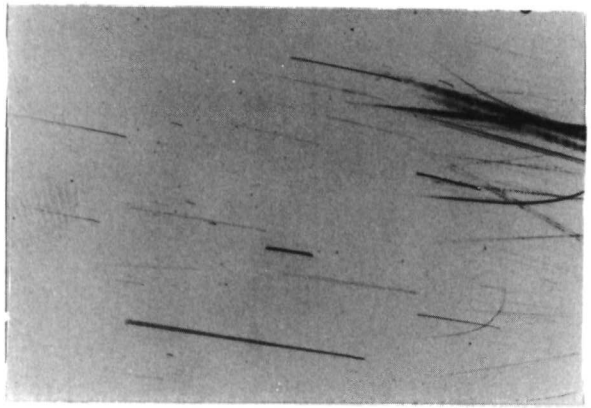

1 SECOND

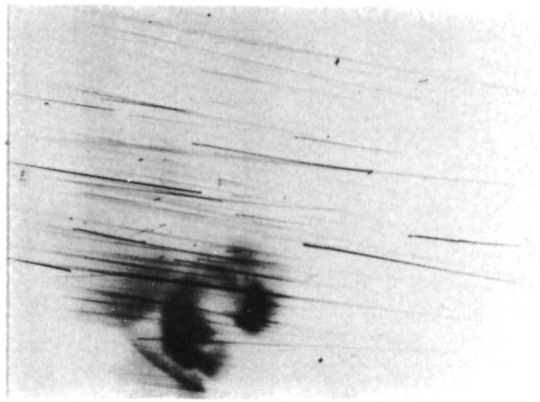

20 SECONDS

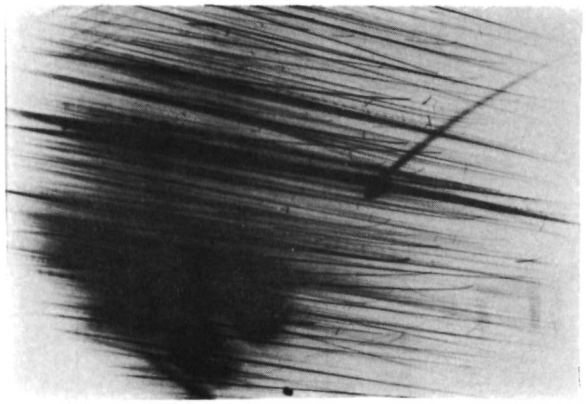

60 SECONDS

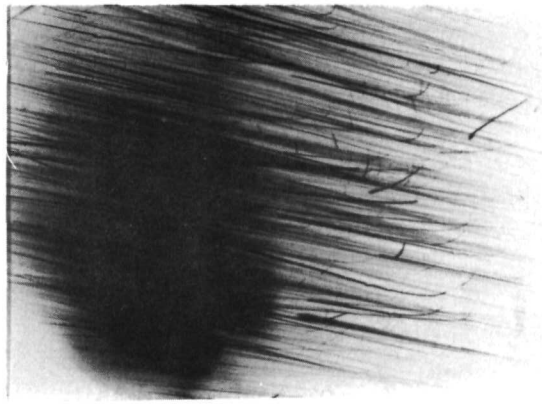

100 SECONDS

Figure 9. Fourth photographic sequence for frames 12 through 15.

astronaut looking out window 4. The sun is below the lower left corner, approximately 8 o'clock. The liquid vents are also located to the left and behind the astronaut at approximately 10 o'clock. Since the astronaut sits with his head in the -Z direction, up is in the direction of the south celestial pole.

Frame 1 (1-sec exposure not shown) had a band of stray light on the right side, very much like that seen in frame 5 (1-sec exposure, 1.5 minutes after dump). A few bright objects could be seen by microscopic examination of the negative, but without identifying star fields it is difficult to determine if these are actually the brighter stars, particles in the vicinity of the spacecraft, or artifacts in the film.

Frame 2 (20-sec exposure not shown) was almost identical with frames 3 and 4 except that it is much fainter. Only the brighter stars were readily apparent in the print; however, microscopic examination of the negative reveals star images as faint as $m_v = 5.6$, which is slightly better than the estimated plate limit (Appendix A).

Frames 3 and 4 are shown in Figure 6. The most easily recognized starfield feature is the group consisting of g, h, i, and k Centarus at the top of the frame. The brighter stars flanking this group are π and γ Hydra and Θ Centarus. Figure 10 shows a star chart [5] of this region. Table 1 gives data pertinent to the stars in the field taken from Smithsonian tables [6]. The star brightness is given in terms of visual magnitude. Because of the blue cut-off in the spacecraft window at 4500 Å, the photographic response is not significantly different from visual response. This is evident from the fact that g Centarus is an M star which has a color index of 1.68, whereas i Centarus is an F5 star with a color index of 0.48. Both stars have the same visual magnitude, but, photographically, i should be 1.2 magnitude brighter than g. It may be seen from the photographs that the two are practically the same brightness; therefore, the visual magnitudes seem more appropriate for comparison.

A number of other star-like images may be seen in frames 3 and 4 that appear in the same location in the two frames. These are obviously neither stars nor particles in the vicinity of the spacecraft. Since the exposure was long compared to the time between frames, particles in different locations in successive frames would have to show considerable motion in the frame, which they do not. These are undoubtedly artifacts produced in the reproduction process. The prints were made from second generation negatives and in the multiple printing processes dust or other sources of noise have ample opportunities to enter the system.

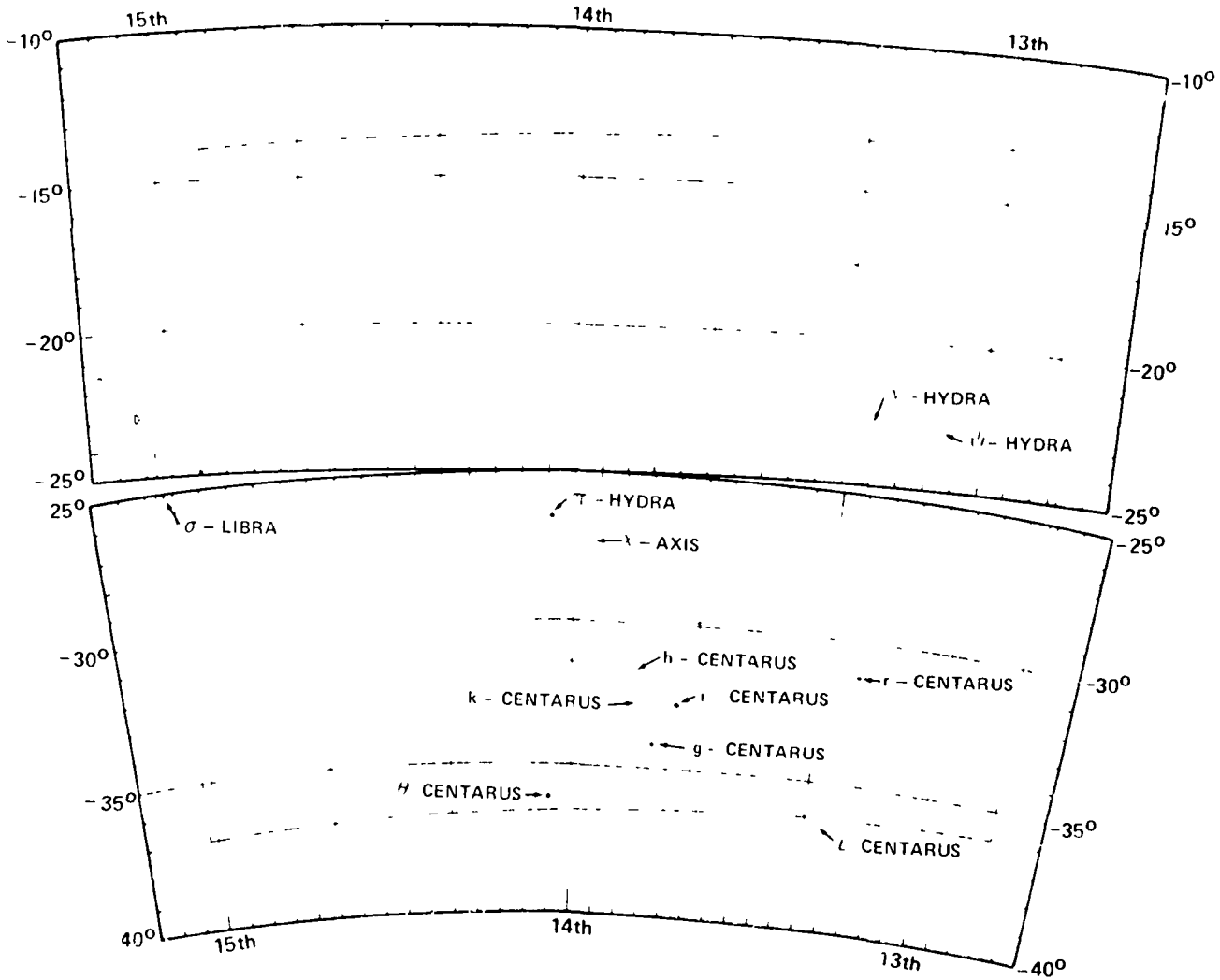

Figure 10. Star chart of the region photographed. (The indicated field of view is that seen in Figure 6. Since this is the southern hemisphere, the star field shown here is inverted relative to that photographed.)

TABLE 1. IDENTIFIABLE STARS IN STAR FIELD

Star	m_v	Spectral Class	R.A.	dec.
θ Centarus	2.3	KO	14:03:43	-36° 07'
h Centarus	4.8	B5	13:50:19	-31° 40'
k Centarus	4 7	B5	13:48:56	-32° 44'
ι Centarus	4.4	F5	13:42:50	-32° 47'
g^2 Centarus	4.4	M_B	13:46:32	-34° 12'
r Centarus	5.4	KO	13:14:06	-31° 15'
y Centarus	5.6	F2	13:50:36	-35° 25'
He24 Centarus	5.2	AO	13:44:00	-36° 00'
Unnamed	6.5	GO	13·46:32	-34° 12'
π Hydra	6.3	KO	13:50:57	-35° 04'
γ Hydra	3.5	KO	13:03:31	-26° 27'
ψ Hydra	3.3	G5	13:16:11	-22° 54'
	5.1	KO	13:06:21	-22° 51'

Figures 11 and 12 are photomicrographs of the second generation negatives in the vicinity of g, h, ι, and k Centarus. The faint smudge in line with g and ι Centarus appears to be the remnant of Nova 1895, Z 5253. The faint smudge to the right of ι Centarus is probably the variable star t Centarus. Figure 13 shows this region extracted from the Norton Star Atlas [7]. The faint stars in Figure 12 between g and Θ Centarus appear to be y and z Centarus, He 24, and the faint unnamed neighbor of g Centarus. These stars are very close to the computed plate limit of 6.8 magnitude based on threshold sensitivity. (See Appendix A.)

The smudges in frames 3 and 4 appear to be internal reflections. Some out-of-focus detail may be seen in these smudges. Since the camera was focused at infinity, this out-of-focus image must have been close to the camera, probably on the window. Whether the light responsible for these reflections leaked through the dark hood or was incident from the spacecraft exterior has not been determined. Since moonlight was incident on the window opening, it is not inconceivable that this could have been caused by diffracted or scattered moonlight from the window opening. If this were light scattered from a contamination cloud, one would not expect to see a localized smudge with out-of-focus detail. The darkening along the bottom edge is probably moonlight reflected from the lower edge of the window. The apparent darkening of the background of frames 3 and 4 is an artifact of the multiple replication. An isodensitracer plot of the original negatives (Fig. 14) shows only base fog in this region.

DENSITOMETRY

To investigate the reciprocity behavior of SO164 film, a series of D versus log E curves at the exposure times used in the experiment was run by the Photographic Technology Division, Manned Spacecraft Center [8]. The results are shown in Figure 15.

The intensity of the detector I is related to the brightness of the cloud B by

$$I = B\omega \qquad (1)$$

where ω is the field of view of the detector. In terms of solar brightness $B_{\odot}$, given by Allen [9] as 2.02×10^9 lumen/m^2/Sr,

Figure 11. Photomicrograph of the group g, h, i, and k Centarus.

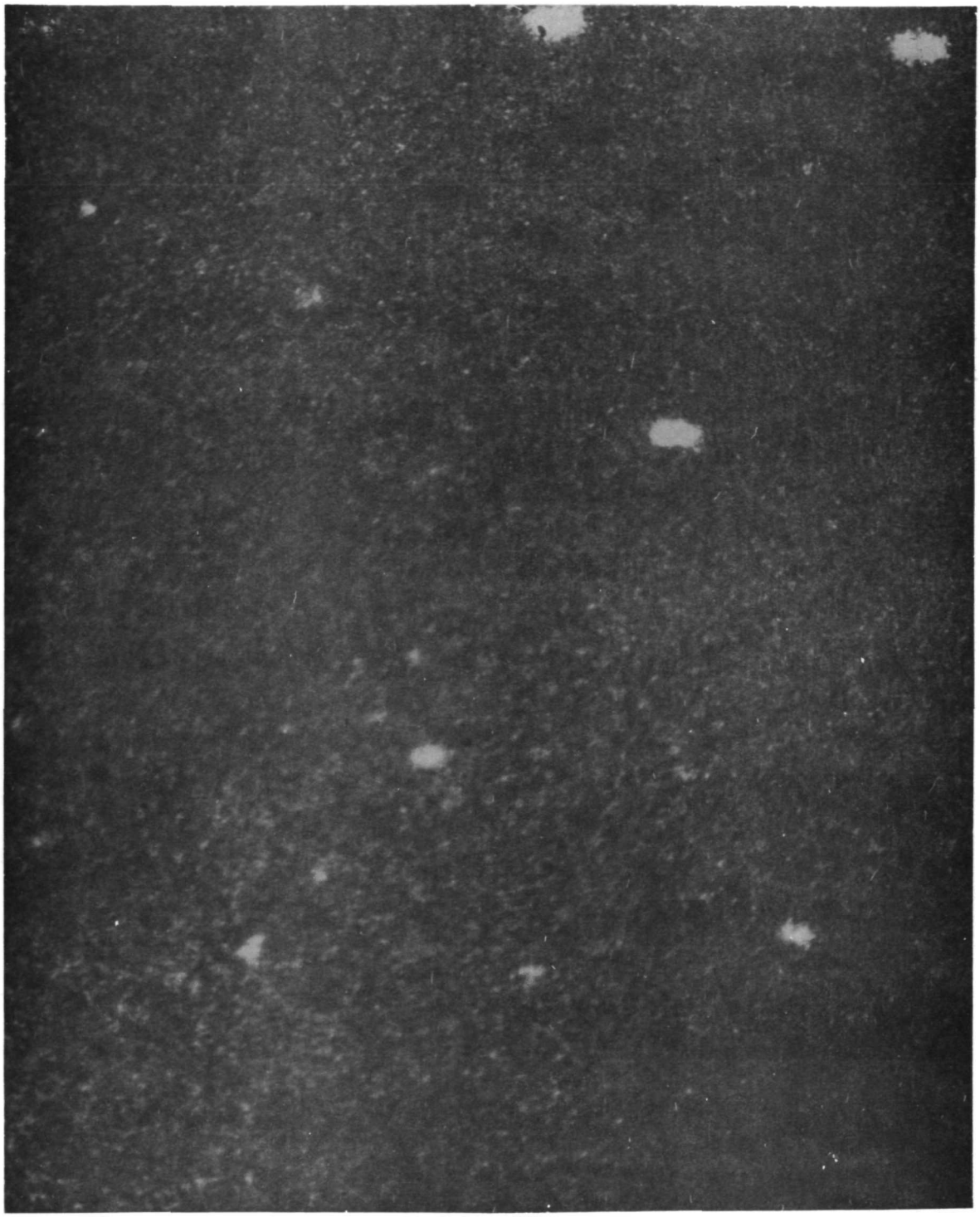

Figure 12. Photomicrograph of region between g, i, and k Centarus (upper right) and θ Centarus which is out of the field beyond the lower left corner.

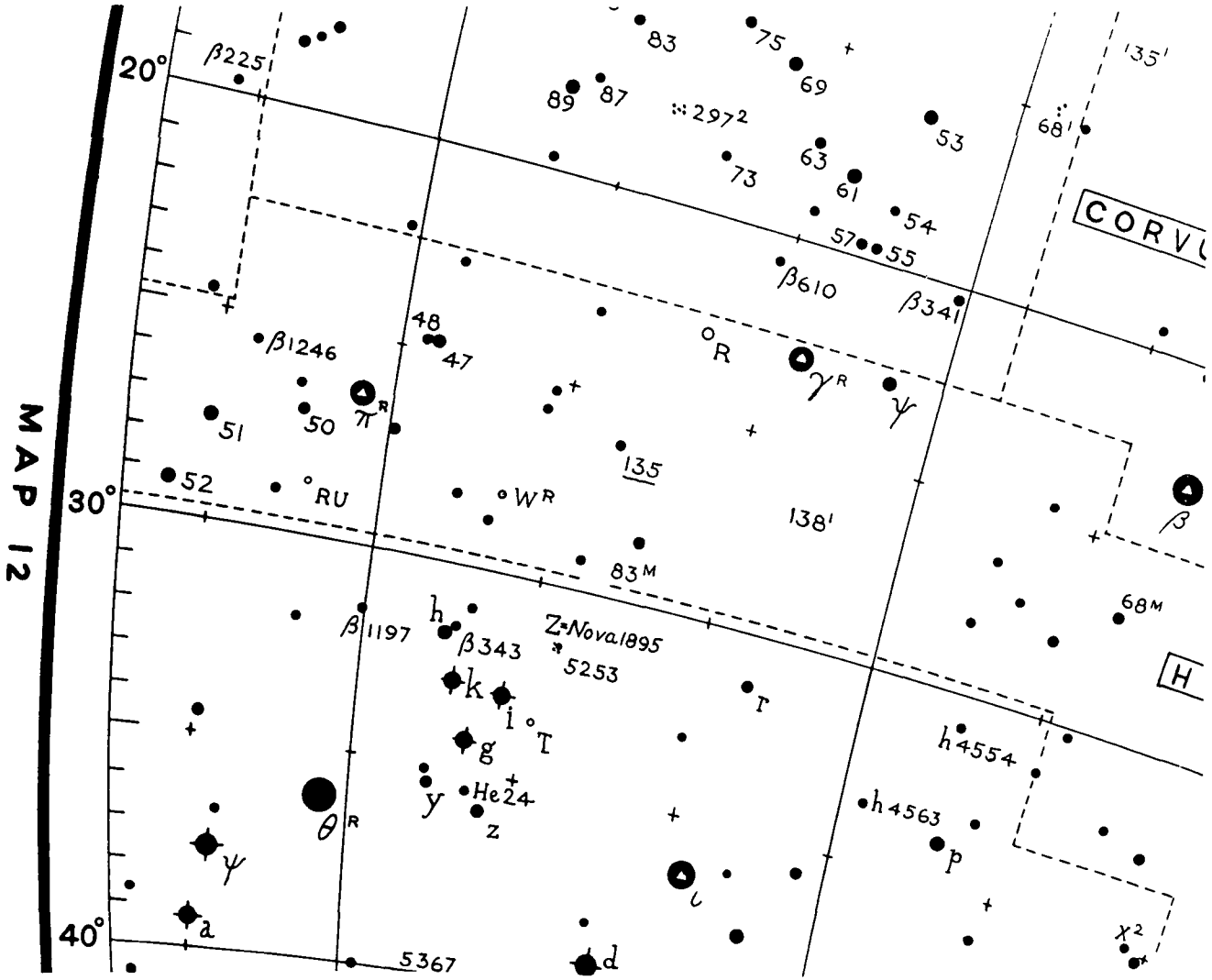

Figure 13. Star map from Norton Star Atlas showing region photographed by Apollo 15.

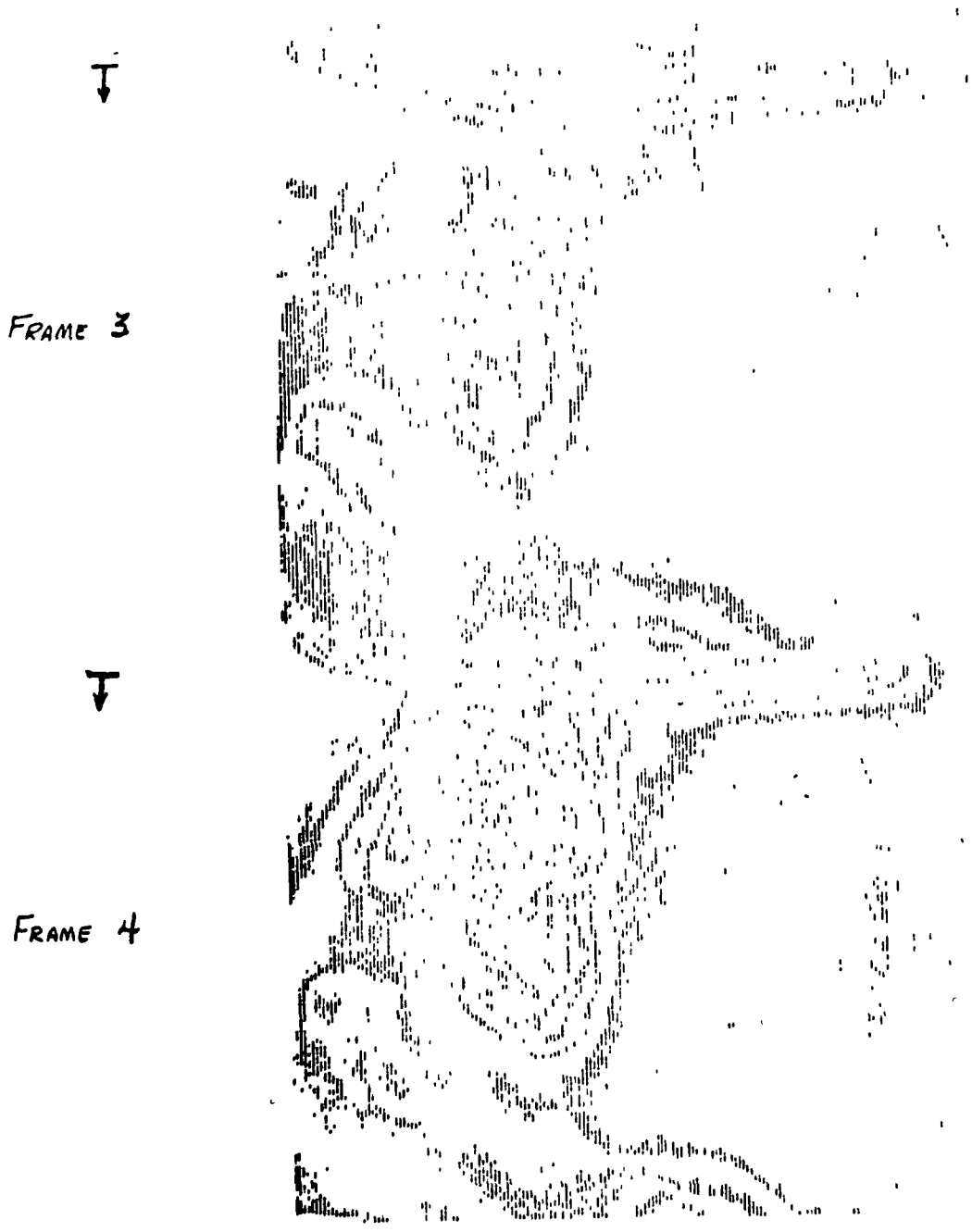

Figure 14. Isodensitracer plots of frames 3 and 4. (These plots were made with the negative right-side-up; therefore, there is right-left reversal relative to Figure 6. The scanning spot was 24 x 30μ with 50-μ spacing between scan lines. The density increment is 0.0188.)

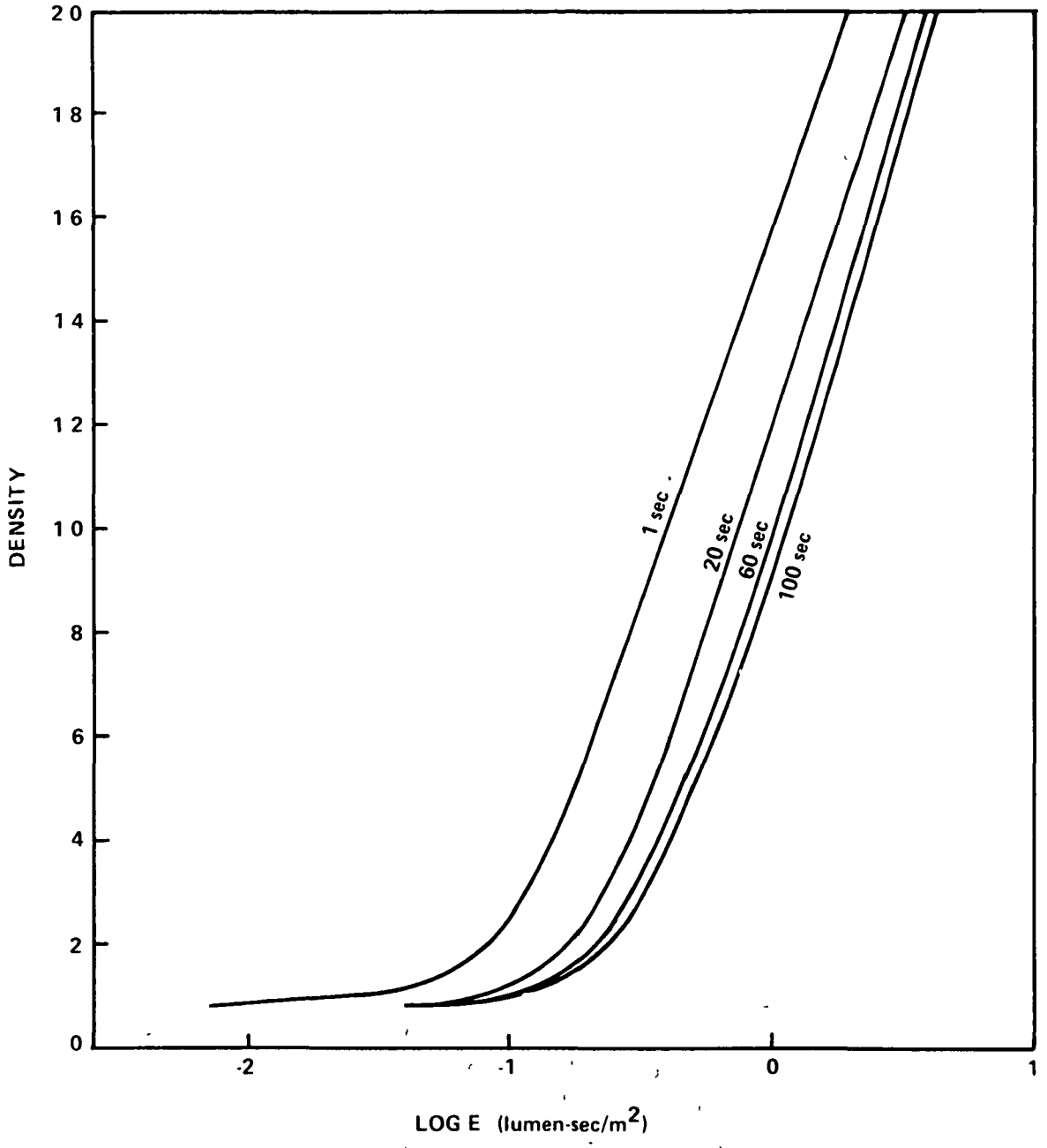

Figure 15. D versus log E plots for SO164 film at exposures of 1, 20, 60, and 100 sec.

$$\frac{B}{B_{\odot}} = \frac{I\,(\text{lumens/m}^2)}{\omega\ (\text{sterad})\ 2.02 \times 10^9\ (\text{lumens/m}^2/\text{sterad})} \quad . \tag{2}$$

The intensity at the film plane is

$$I_{film} = I_o \frac{\pi d^2}{4} \frac{T}{F^2\omega} = I_o \frac{\pi}{4} \frac{T}{f^2\omega} \tag{3}$$

where I_o is the intensity incident on the lens, $\pi d^2/4$ is the collecting area, T is the transmission, F is the focal length, $F^2\omega$ is the area on the film subtended by ω, and f is the f-number, F/d. Combining equation (3) with equation (2),

$$\frac{B}{B_{\odot}} = \frac{4\,f^2\,I_{film}}{\pi\ T\ 2.02 \times 10^9} \quad . \tag{4}$$

The I_{film} is obtained by dividing the exposure inferred from the measured density by the exposure time.

The published transmission data for the spacecraft window plus the 80-mm planar f/2.8 lens [10] indicate a transmission of approximately 0.69 for wavelengths longer than 450 nm at normal incidence, and a drop to approximately 0.48 at a 45-deg incidence. The 80-mm lens has an average transmission of 0.8. The 18-mm lens used for this experiment is rated at f/0.9 and T/1.0, which implies a transmission of 0.9. The overall transmission, including the 45-deg mirror, is estimated to be 0.75 for normal incidence on the window. The transformation from density to $B/B_{\odot}$ is shown in Figure 16 for f/0.9 and T = 0.75. However, the window is sloped at approximately 30 deg to the optical axis of the camera. The vertical field of view is 23.5 deg. Therefore, the top of the frame corresponds to an angle of incidence of 18.25 deg, and the bottom corresponds to 41.75 deg. It is assumed that the transmission of the window follows a cosine behavior; this is consistent with the measured data at 0 and 45 deg. Therefore, the transmission varies from

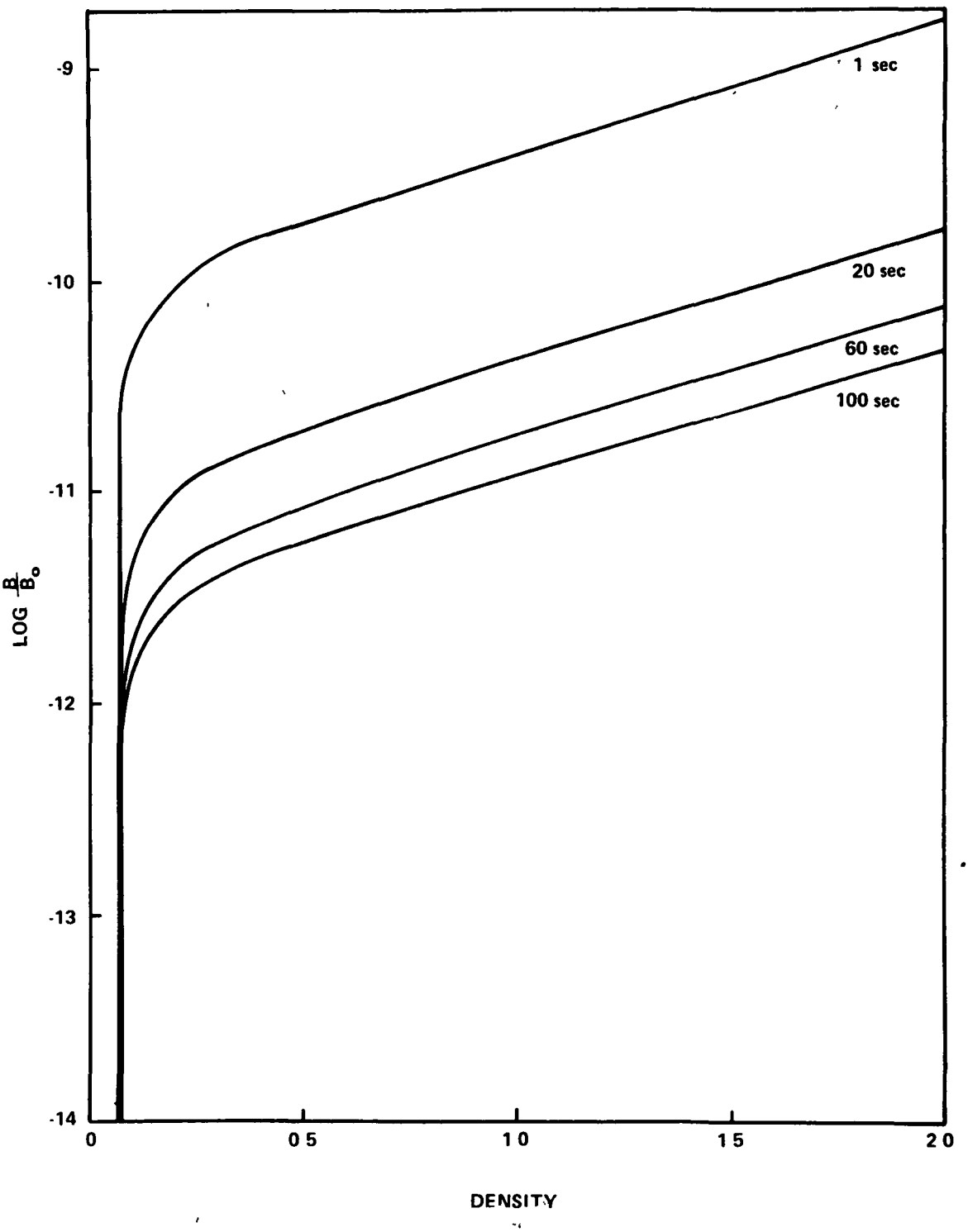

Figure 16. $B/B_{\odot}$ inferred from density measurements on SO 164 film exposed on Apollo 15 assuming transmission factor of 0.75.

0.71 at the top of the frame to 0.56 at the bottom. The $B/B_{\odot}$ values read from Figure 16 must be divided by the cosine of the angle of incidence to correct for this effect.

All densitometry was performed on original film. Frames 3 and 4 were measured with a MacBeth instrument with a 4-mm spot size. This size spot subtends a 12.8-deg field of view (0.039 sterad), which gives an integrated measurement of the sky background plus any particles or stars that may be in the field. This is similar to the information that will be obtained by the T-027 photometer to be flown on Skylab. Three measurements were made on each negative: one in the center, one halfway between the center and the edge in the +Y direction, and one between the center and edge in the -Y direction. The ±Y readings correspond to angles of ±7.9 deg relative to the X axis.

The results are shown in Tables 2 and 3. The first two frames exhibited only base fog on the +Y side. This sets an upper limit of $B/B_{\odot} = 10^{-12.3}$ on the cloud brightness at $\Theta_{\odot} = 91$ deg. It may be seen that the 0 and -Y readings will be influenced by the internally reflected light apparent in these frames. Even if this peculiar image was a contamination cloud, its brightness is $10^{-11.71} B_{\odot}$ or less at $\Theta_{\odot} = 75$ deg.

These results are compared with estimates of the contamination cloud brightness made by Newkirk in Figure 17 and Kovar et al. in Figure 18. It is unfortunate that the upper limits set by this measurement are still slightly above the corona and zodiacal light brightness at these angles. Also, they are above the estimates made by Newkirk of the contamination cloud surrounding Apollo, but below the estimates made by Kovar et al. However, it can be stated with certainty that any inability of astronauts to see stars must be because of reasons other than a contamination cloud.

The remaining frames are after the dump, and the brightness data may be used to infer the clearing time. In this analysis, two types of densitometry were used. The 4-mm spot measures the total integrated light from a 12.8-deg field of view, as before, and is indicative of the total scatter present from the ice crystal produced by the dump. In addition, a microdensitometer with a 25- by 50-μ slit was used to measure the background of unresolved particles by looking between the resolved particle tracks. Its field of view is 0.08×0.16 deg or 4×10^{-6} steradians.

TABLE 2. DENSITIES (4-mm SPOT)

Group	Frame	Figure	Exp. (sec)	+Y	O	-Y
Before	3	6	60	0.06	0.11	0.08
Dump	4	6	100	0.06	0.11	13
1.5 to 5 Min	5	7	1	1.17	0.17	0.17
After Dump	6	7	20	1.26	1.16	1.00
	7	7	60	0.72	1.26	1.13
	8	7	100	0.85	1.38	1.41
8 to 10 Min	9	8	20	0.12	0.20	0.25
After Dump	10	8	60	0.14	0.25	0.34
	11	8	100	0.80	1.14	1.25
25 to 28	12	9	1	0.12	0.06	0.06
Min After	13	9	20	0.065	0.11	0.12
Dump	14	9	60	0.25	0.58	0.65
	15	9	100	0.24	0.69	0.69

TABLE 3. LOG B/B_O (4-mm SPOT)

Group	Frame	Figure	Exp. (sec)	+Y	O	-Y	Time After 272:00:00 GET (min)
Before Dump	3	6	60	< -11.93	-11.63	-12.03	1.3
	4	6	100	< -12.33	-11.83	-11.71	3
1.5 to 5 Min After Dump	5	7	1	- 9.21[a]	-10.05	-10.07	28.5
	6	7	20	-10.17	-10.23	-10.33	29.3
	7	7	60	-10.87	-10.53	-10.61	30.3
	8	7	100	-11.13	-10.65	-10.63	32
8 to 10 Min After Dump	9	8	20	-11.21	-10.98	-10.73	34.3
	10	8	60	-11.49	-11.26	-11.15	35.3
	11	8	100	-11.01	-10.89	-10.73	37.0
25 to 28 Min After Dump	12	9	1	-10.21	< -11	< -11	52
	13	9	20	< -11.73	-11.27	-11.21	52.3
	14	9	60	-11.26	-11.08	-10.92	53.3
	15	9	100	-11.43	-11.07	-11.07	55

a. Probable light leak.

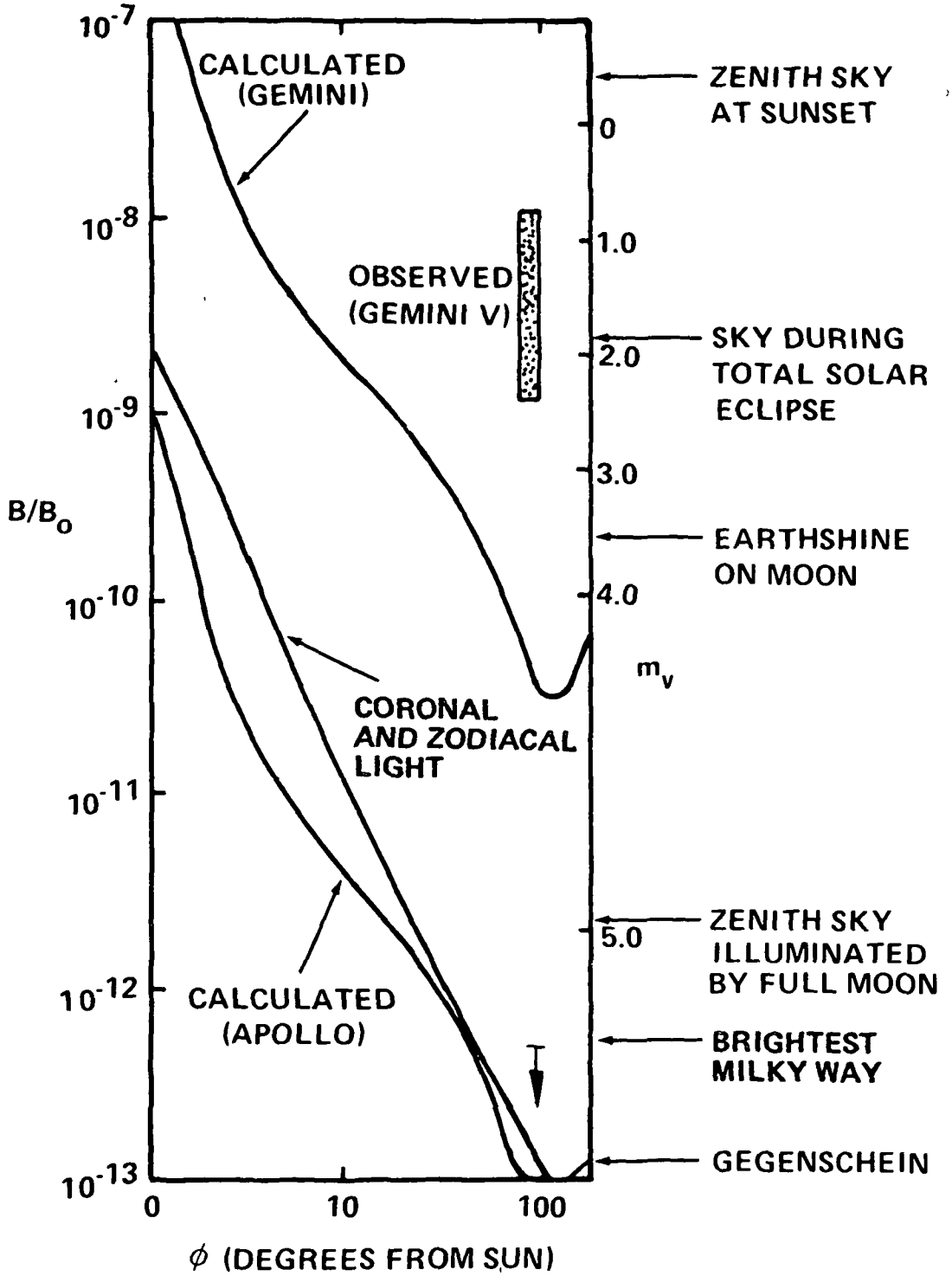

Figure 17. Upper limit of contamination cloud brightness compared with zodiacal light background and estimated background brightness of Newkirk.

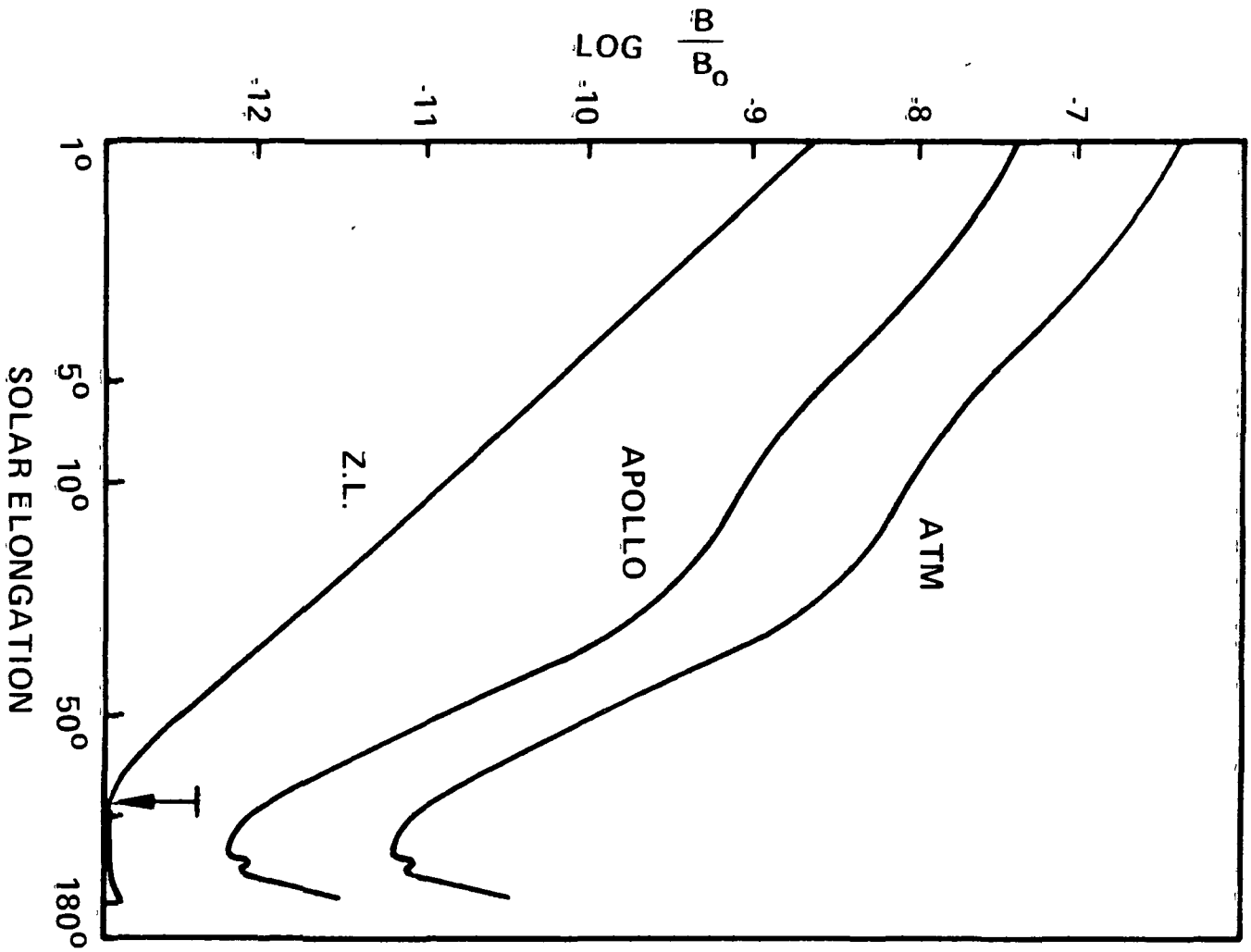

Figure 18. Upper limit of contamination cloud brightness compared with estimated background brightness of Bonner, Kovar, and Kovar.

A plot of both results as a function of time is shown in Figure 19. It is interesting to note that the scattered intensity decays rapidly as the debris cloud apparently moves away from the spacecraft. However, abrupt increases in cloud intensity followed by rapid decays are noted. It is believed that such increases result from fresh material leaving the spacecraft, which was confirmed by astronaut observations. This can happen because the dump system has approximately 4 meters of line between the valve and the dump nozzle. It is known that freezing occurs in and around the nozzle exit; therefore, it is not unlikely that substantial vapor and ice may be trapped in the line as the nozzle freezes, and subsequently released as the freeze plug sublimes. This effect can be clearly seen by comparing the 60-sec exposure with the 100-sec exposure taken 10 min after dump (Fig. 8). Notice that many more particles appear to be near the window in the 100-sec exposure, as evidenced by their long out-of-focus tracks. Apparently, these particles were just released by the process described above.

LIGHT SCATTERED FROM THE PARTICLE CLOUD

Let the instrument have a field of view of ω steradians. The area intercepted by this field at distance r is ωr^2. The number of particles in the volume element subtended by the field of view at distance r is

$$N(r)\ \omega\ r^2\, dr \tag{5}$$

where $N(r)$ is the number density of particles.

Let a beam with intensity $I_\odot$ be incident on a particle with differential cross section $d\sigma/d\Omega$. The number of photons per sec scattered into a solid angle $\Delta\omega$ is

$$N = I_\odot \frac{d\sigma}{d\Omega} \Delta\omega \ . \tag{6}$$

By definition of solid angle, $\Delta\omega = \Delta A/r^2$. The number of photons scattered into ΔA, or the scattered intensity, I_s, becomes

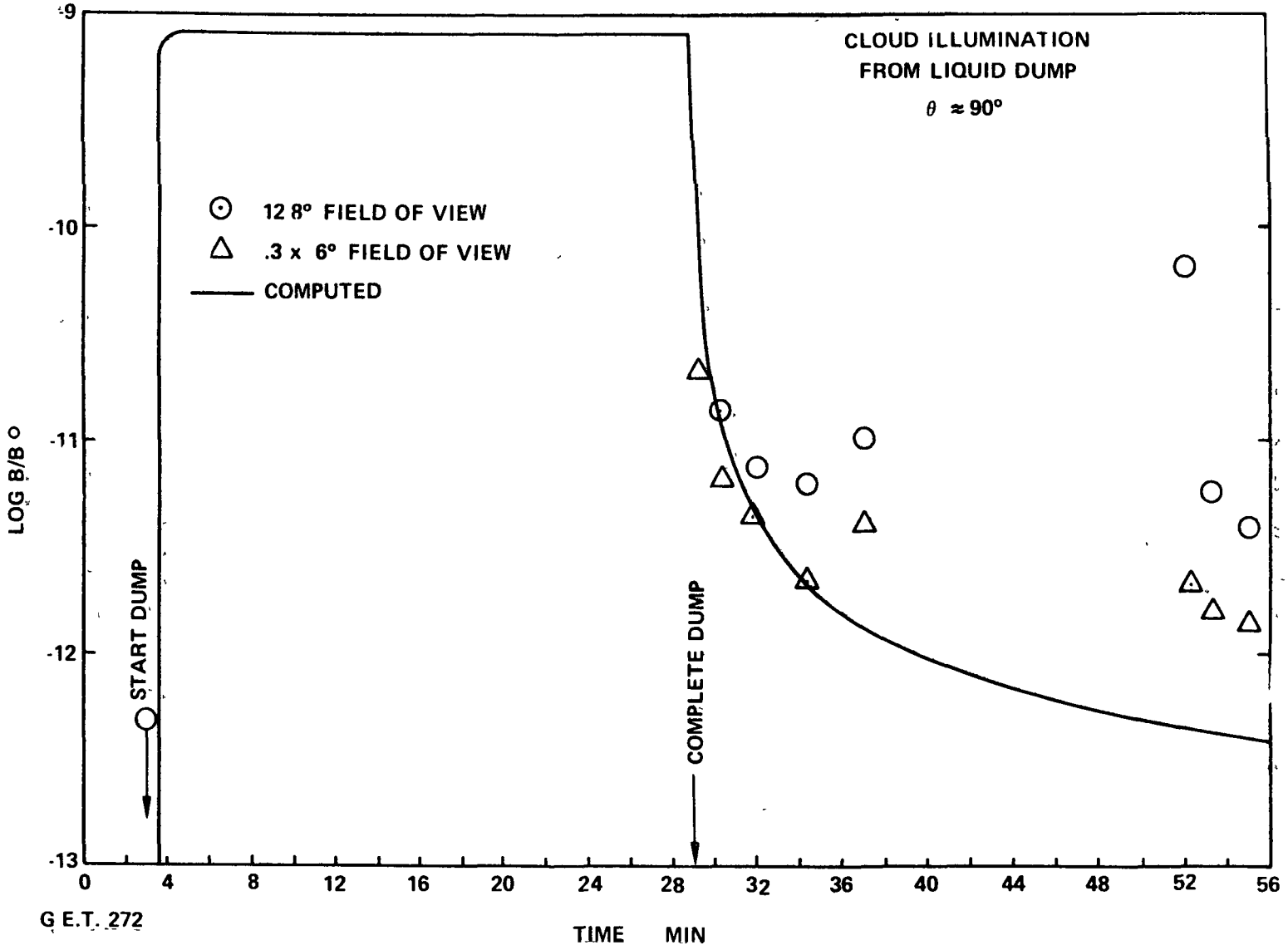

Figure 19. Clearing times for waste dump debris cloud.

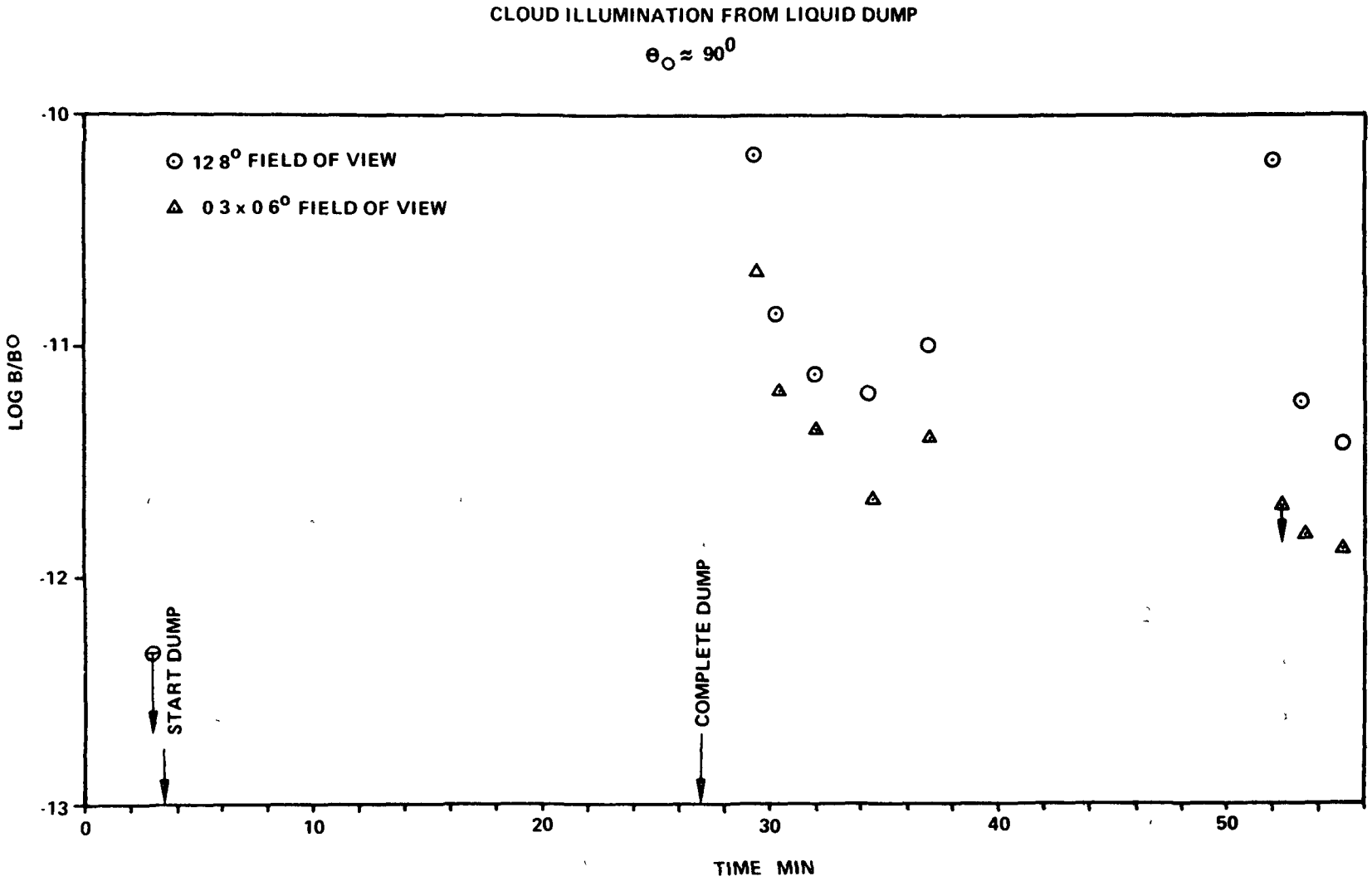

Figure 19. (Concluded).

$$I_s = \frac{N}{\Delta A} = \frac{I_\Theta}{r^2} \frac{d\sigma}{d\Omega} \quad . \tag{7}$$

Integrating this scattered intensity per particle over the size distribution of particles per unit volume and then integrating over the column gives the total intensity received, which is

$$I = I_\Theta \omega \int_{r_o}^{\infty} dr \int_{o}^{\infty} da\, N_{ra}(r, a) \frac{d\sigma}{d\Omega} \quad . \tag{8}$$

Assuming the spatial distribution is independent of size distribution, $N_{ra}(r, a)$ can be written $N_a(a)\, N_r(r)$ and the integral may be written

$$\int_{r_o}^{\infty} N_r(r)\, dr \int_{o}^{\infty} N_a(a)\, da = N_c \tag{9}$$

where N_c is the column density.

The brightness becomes

$$\frac{B}{B_\Theta} = \frac{\omega_\Theta}{\omega} \frac{I}{I_\Theta} = \omega_\Theta N_c \left\langle \frac{d\sigma}{d\Omega} \right\rangle \quad . \tag{10}$$

SCATTERING CROSS SECTION

For very small particles, $a << \lambda$, the differential cross section is given by Rayleigh theory [11],

$$\frac{d\sigma}{d\Omega} = 8\pi^4 \frac{a^6}{\lambda^4} \left| \frac{n^2 - 1}{n^2 + 2} \right|^2 (1 + \cos^2 \Theta) \quad . \tag{11}$$

For ice, $n = 1.33$ and the above becomes

$$\frac{d\sigma}{d\Omega} = 10.32\ \pi a^2 \left(\frac{a}{\lambda}\right)^4 \quad (1 + \cos^2 \Theta) \quad . \tag{12}$$

For $a >> \lambda$, the scattering is dominated by diffraction [12] and

$$\frac{d\sigma}{d\Omega} = \pi^2 \frac{a^4}{\lambda^2} \left| \frac{2 J_1 (x)}{x} \right|^2 \tag{13}$$

where

$$x = \frac{2 \pi a}{\lambda} \sin \Theta \quad .$$

For $\Theta >> 0$ and since $\Theta >> \lambda$, the asymptotic approximation for the Bessel function [13] may be used; i.e.,

$$J_1 (x) \underset{x>>1}{\rightarrow} \left| \frac{2}{\pi x} \right|^{1/2} \cos x \quad . \tag{14}$$

Since x is large, the average of a cycle may be approximated by

$$\int_x^{x+2\pi} \left[\frac{2 J_1 (x)}{x}\right]^2 dx \cong \frac{8}{\pi |x|^3} \int_x^{x+2\pi} \cos^2 x\, dx = \frac{4}{\pi |x|^3} \quad . \tag{15}$$

Thus,

$$\frac{d\sigma}{d\Omega} = \frac{\pi^2 a^4}{\lambda^2} \frac{4}{\pi |x|^3} = \frac{a\lambda}{2\pi^2 |\sin^3 \Theta|} \quad . \tag{16}$$

For the case where $a \approx \lambda$, the complete Mie theory [14] must be used. The differential cross section is expressed by

$$\frac{d\sigma}{d\Omega} = \frac{\lambda^2}{8\pi a^2} (i_1 + i_2) \tag{17}$$

where i_1 and i_2 are infinite series of linear combination of Ricatti-Bessel and Ricatti-Hankel functions and their derivatives, multiplied by derivatives of Legendre polynomials. Tabulations of the quantities are available [15]. Figure 20 shows the differential cross section normalized by the geometric cross section for $\Theta = 90$ deg. Very close agreement between the Mie theory and diffraction theory is seen until the intersection of the Rayleigh theory with the asymptotic approximation. For order of magnitude calculations, and since the shape of the particles is unknown, the differential cross section given by the asymptotic approximation will be adopted for $a > a_1$ where a_1 is the intersection of the two curves.

The integral

$$\int_0^\infty N_a(a) \frac{d\sigma}{d\Omega} da \cong \frac{\lambda \bar{a}}{2\pi^2 |\sin^3 \Theta|} \tag{18}$$

where $\bar{a}$ is the average radius. Finally,

$$\frac{B}{B_\Theta} = \frac{\omega_\Theta N_c \lambda \bar{a}}{2\pi^2 |\sin^3 \Theta|} \tag{19}$$

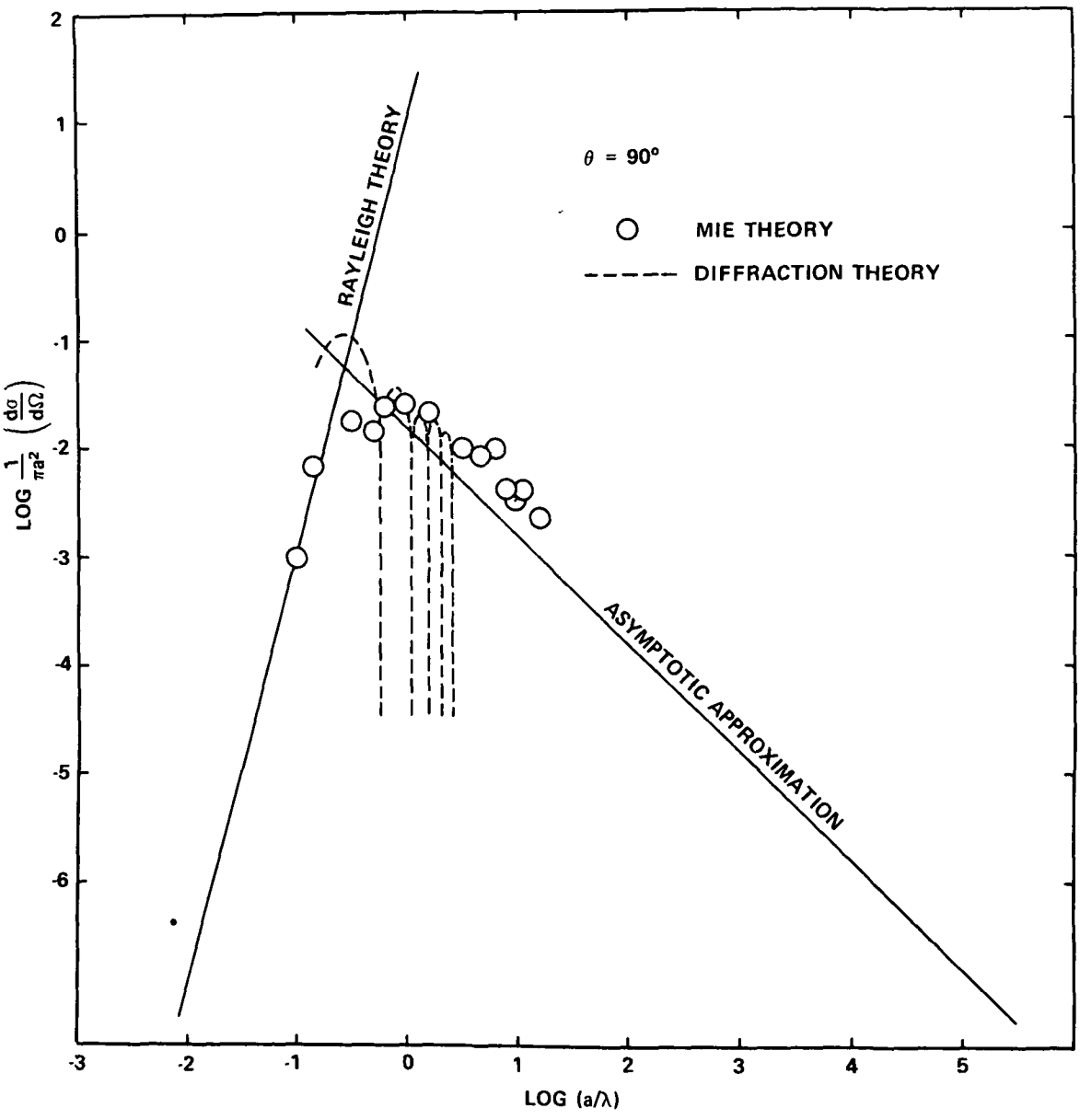

Figure 20. Comparison of the scattering cross section computed from Rayleigh theory, Mie theory, diffraction theory, and the asymptotic approximation for a sun angle of 90 deg.

COLUMN DENSITIES

The column density is obtained by integrating the number density $N_r(r)$ along the sight vector. $N_r(r)$ is obtained by dividing the directional flux ϕ by ν, the average radial velocity.

For a plume, the directional flux is a function of r', the distance along the radius from the nozzle, and Θ', the angle r makes with the plume axis. Let $\vec{r}_o$ be a vector from the nozzle to the sight vector making a right angle with the sight vector. Let $\vec{r}_1$ be a vector from the sight vector to the nozzle making a right angle with the nozzle axis. At a distance x from $\vec{r}_o$ along the sight vector, the distance to the nozzle is

$$r'^2 = r_o^2 + x^2 \quad . \tag{20}$$

Assume the flux distribution is given by

$$\phi(\Theta', r') = \frac{\dot{N}_T \cos \Theta'}{\pi r'^2} \quad ; \quad 0 \leq \Theta' \leq \pi/2 \tag{21}$$

where $\dot{N}_T$ is the rate at which particles are ejected. The flux at any x along the sight vector is given by

$$\phi(x) = \frac{\dot{N}_T}{\pi} \frac{\cos \gamma \left(x - \sqrt{r_1^2 - r_o^2} \right)}{\left(r_o^2 + x^2 \right)^{3/2}} \quad ; \quad x \geq \sqrt{r_1^2 - r_o^2} \tag{22}$$

where γ is the angle between the vent axis and the line of sight. Assuming ν is constant, this may be integrated to give

$$N_c = \int_{\sqrt{r_1^2 - r_o^2}}^{\infty} \frac{\phi(x)}{v}\, dx = \frac{\dot{N}_T \cos\gamma}{\pi v r_o^2} \left(r_1 - \sqrt{r_1^2 - r_o^2} \right) . \tag{23}$$

This gives the steady state column density. This assumes that the viewing point is behind the intersection of r_1 and the sight vector. If not, use equation (24). When $\dot{N}_T$ is first turned on, the contributions will come only from values of x less than $\sqrt{(vt_1)^2 - r_o^2}$ where t_1 is the time since initiation of the vent. Similarly, when the vent is terminated, the contributions cease at values of $x = \sqrt{(vt_2)^2 - r_o^2}$ where t_2 is time after termination.

Integrating between these limits,

$$N_c = \frac{\dot{N}_T \cos\gamma}{\pi v} \left[\frac{1}{r_r} - \frac{1}{r_f} - \left(\frac{\sqrt{r_1^2 - r_o^2}}{r_o^2} \right) \left(\frac{\sqrt{r_f^2 - r_o^2}}{r_f} - \frac{\sqrt{r_r^2 - r_o^2}}{r_r} \right) \right] \tag{24}$$

where $r_f = vt_1$, r_1', r_1 whichever is greater, and $r_r = vt_2$, r_1', r_1 whichever is greater, where r_1 is the distance from the vent to the viewing point.

For Apollo, looking along the x axis, $\gamma = 57.477$ deg, $r_o = 2.35$ m, and $r_1 = 3.38$ m. Ground-based photographs [4] of dump-cloud expansion indicate an average v of 6 m/sec. The column densities looking out through window 4 along the x axis are given in Table 4.

To obtain the $\dot{N}_T$, simply divide the mass flow rate of the dump $\dot{M}$ by the average mass per particle. Therefore,

TABLE 4. COLUMN DENSITIES

Time After Dump Start	$N_c/\dot{N}_T$ (m^2 sec)	$B/B_\odot$
30 Sec	4.752×10^{-3}	6.3×10^{-10}
1 Min	4.831×10^{-3}	6.4×10^{-10}
20 Min	4.906×10^{-3}	6.5×10^{-10}
∞	4.910×10^{-3}	6.5×10^{-10}
Time After Dump Stop		
0	4.910×10^{-3}	6.5×10^{-10}
30 Sec	1.574×10^{-4}	2.08×10^{-11}
1 Min	7.895×10^{-5}	1.04×10^{-11}
5 Min	1.583×10^{-5}	2.10×10^{-12}
10 Min	7.921×10^{-6}	1.05×10^{-12}
30 Min	2.641×10^{-6}	3.49×10^{-13}

$$\frac{B}{B_\odot} = \frac{\omega_\odot \lambda \dot{M}}{2\pi^2} \left(\frac{N_c}{\dot{N}_T}\right) \left(\frac{\bar{a}}{\bar{m}}\right) \quad . \tag{25}$$

Taking $\omega_\odot = 6 \times 10^{-5}$ sr, $\lambda = 0.5 \times 10^{-6}$ m, and $\dot{M} = 10^{-2}$ kg/sec,

$$\frac{B}{B_\odot} = 1.52 \times 10^{-14} \quad \frac{N_c}{\dot{N}_T} \quad \frac{\bar{a}}{\bar{m}} \quad .$$

Choosing $\bar{a}/\bar{m}$ 8.7×10^6 m/kg gives an acceptable fit to the first several data points. Since fresh material left the spacecraft at around 36 minutes after dump, agreement would not be expected beyond this point. The value for $\bar{a}/\bar{m}$ corresponds to a particle 10.5 microns in diameter.

The maximum cloud brightness would be obtained if the entire mass were divided into particles with radii of 0.137 micron, which represents the intersection of the Rayleigh theory with the asymptotic approximation. Such a distribution would result in a steady state cloud brightness of nearly 10^{-6} $B_\odot$, which would correspond to the daylight sky. This is more than three orders of magnitude greater than required to match the observed brightness.

A power law size distribution of the form $N_a(a) \sim a^{-\beta}$ is often used to describe aerosols. A typical value for β is four. If such a distribution is assumed from molecular sizes up to the minimum size for which individual particles can be discerned (taken to be $a = 1.75 \times 10^{-4}$ m), 49.5 percent of the mass of the particles will be distributed in sizes less than 0.137 micron. For this group, the average cross section $\langle d\sigma/d\Omega \rangle = 2.6 \times 10^{-24}$ m^2 and the average mass $\langle m \rangle = 1.7 \times 10^{-25}$ kg. The brightness contribution from this group is from equation (10):

$$\frac{B}{B_\odot} = \omega_\odot \left(\frac{N_c}{\dot{N}_T}\right) \frac{\dot{M}}{\langle m \rangle} \left\langle \frac{d\sigma}{d\Omega} \right\rangle$$

$$= \frac{6 \times 10^{-5} \, (4.91 \times 10^{-3}) \, (0.495) \, (10^{-2}) \, (2.6 \times 10^{-24})}{1.7 \times 10^{-25}}$$

$$B = 2.2 \times 10^{-8}\ B_{\odot} \quad . \qquad (26)$$

For the group larger than 0.137 micron but smaller than 1.75×10^{-4} m, the average radius is 2.05×10^{-7} m and the average mass is 2.31×10^{-16} kg. This contribution to cloud brightness is from equation (25): $B = 6.62 \times 10^{-8}\ B_{\odot}$. Again, the total contribution is more than two orders of magnitude greater than required.

Since larger particles are known to exist in the dump cloud, and since the assumption that the power law distribution function extended to the smaller sizes produces much greater brightness than observed, a more reasonable assumption would be to truncate the distribution at some value of a_{min}. For a $\beta = 4$ distribution, this value is $a_{min} = 1.725$ microns. Of course, many other distributions could give the observed results, and the data are not sufficient to establish any particular model. The essential point here is that the cloud produced by water dumping probably consists of particles larger than several microns. Otherwise, the cloud would be considerably brighter than observed.

INDIVIDUAL PARTICLES

The larger particles which appear as individual particles are most likely aggregates of smaller particles or ice crystals with highly irregular surfaces. For this reason they can be considered as Lambertian reflectors with a differential cross section $d\sigma/d\Omega = 2a^2/3$ for $\Theta = 90$. (See Appendix C.) The scattered intensity in terms of stellar magnitudes is given by

$$\frac{I_s}{I_{\odot}} = \frac{1}{r^2}\ \frac{d\sigma}{d\Omega} = 10^{-0.4\,(m_v\ -\ m_{\odot})} \quad . \qquad (27)$$

Since $m_{\odot} = -26.78$ (equivalent to 1.365×10^5 lumens/m^2),

$$m_v = +2.5 \log 3/2 - 26.78 + 5 \log r/a. \qquad (28)$$

The intensity falling on the film is

$$I_{film} = \frac{I_s \pi d^2 T}{4 A_f} \tag{29}$$

where d is the diameter of the objective lens, T is the transmission, and A_f is the area of the image on the film.

For a moving object, this A_f is given by the width times the track length, which is the writing speed W multiplied by the exposure time. The writing speed is related to particle motion by

$$W = \frac{v \sin \alpha F}{r} \tag{30}$$

where F is the focal length and α is the angle between the particle track and the optical axis. For $r >> r_o$,

$$\sin \alpha \simeq \frac{r_o}{r} \quad . \tag{31}$$

Since spacecraft motion and lens aberrations combine to produce a star image which measures approximately 20 μ, the A_f becomes

$$A_f = 2 \times 10^{-7} \quad \frac{v r_o F t}{r^2} \quad . \tag{32}$$

The exposure becomes

$$E = I_{film} t = \frac{I_\odot 2 a^2 \pi d^2 T r^2 t}{r^2 (3)(4) \; 2 \times 10^{-5} v r_o F t} \quad . \tag{33}$$

Using $d = 2 \times 10^{-2}$ m, $F = 1.8 \times 10^{-2}$ m, $r_o = 2.35$ m, $v = 6$ m/sec, $T = 0.65$, and $I_\odot = 1.365 \times 10^5$ lumens/m^2,

$$E = 3.66 \times 10^6 \, a^2 \quad . \tag{34}$$

Assuming a density of 0.1 is required to observe a track, the smallest particle that can be photographed is obtained by setting $E = 0.029$ m-candle-sec (lumen-sec/m^2) which yields

$$a = 8.9 \times 10^{-5} \text{ m} \quad . \tag{35}$$

It is interesting to note that neither the distance nor the exposure time enter this equation. This is because the r^{-2} decrease in intensity is compensated by the same decrease in writing speed. The fact that the tracks appear to be uniform in density even though the particles are moving many meters away from the spacecraft during the exposure bears this out. There is a second order effect which decreases the intensity as the particles recede; i.e., reciprocity failure of the film. As the particles move away, the I_{film} diminishes and the slower the image moves across the film. This increases the effective exposure time, and the film becomes less sensitive because of reciprocity failure. When the particle moves far enough away so that its motion during the exposure time is equal to the width of a star image, it then behaves as a star and its image intensity will diminish with time. This distance is found by equating Wt to the width of a star image and solving for r. (This assumes the spacecraft rates are such that they do not spread the image during the exposure time.)

$$\frac{v \, r_o \, F \, t}{r^2} = 2 \times 10^{-5} \tag{36}$$

for $t = 100$ sec, $r = 1126$ m. The size of particle that could be photographed at this distance is found from equation (34) by setting the required exposure to 0.112 m-candle-sec, which corresponds to a density of 0.1 for a 100-sec exposure. This gives $a = 1.75 \times 10^{-4}$ μ which is equivalent to a 7.7 magnitude star.

Such particles would be extremely difficult to detect on the film, particularly if there is a background from unresolved material. Most of the individual tracks are much more dense than the star images in the field. It is estimated that the readily apparent particles range from $m_v = 3$ to brighter than $m_v = -2$. Such particles would be in the size range from 3 mm to 3 cm in diameter.

PARTICLE TRAJECTORIES

The peculiar particle tracks seen in Figures 8 and 9 are primarily results of vehicle motion. The short curved tracks are stars or particles sufficiently far from the spacecraft so their angular motion is small. The long straight tracks are much closer particles that move through the field of view so rapidly that the spacecraft motion does not affect their image significantly. However, the 1-sec exposure, taken at 25 minutes after dump (Fig. 9), shows several curved trajectories that do not appear to be explainable in terms of vehicle motion. This was a very short exposure; therefore, since the angular rates were never more than 2 deg/minute, the most angular change during the exposure time of 1 sec is 0.03 deg, which represents only 1/1000 of the width of the frame. Second, several particles with perfectly straight-line trajectories definitely begin and end in the field of view. Such particles must obviously have been in the field of view for the entire exposure, and any angular shift should be observed in their track. The only motion allowable that is consistent with a straight track is a rotation about an axis perpendicular to the track. The several tracks that appear curved would require not only unrealistic angular rates, but the angular displacements necessary to obtain the amount of curvature are actually greater than the observed shifts in some of the straight lines that are in the field of view. Therefore, it appears that the particles must actually curve, which implies some external force acting on them.

The radius of curvature of the particle in the lower right corner of frame 12 measured 0.7 mm on the negative. With an 18-mm focal length lens, this corresponds to an actual radius of curvature of 0.04 x, where x is the distance from the particle to the camera. The particle can be no closer than 18 m and produce an in-focus image whose width is equivalent to a star (assumed to be 20 μ). (See Appendix D.) The track length on the film is 2.5 mm. Since this was a 1-sec exposure, the writing speed is 2.5 mm/sec. This requires the particle to have a perpendicular velocity component of at

least 2.5 m/sec. The acceleration required is proportional to the distance of the particle from the camera and is 8.7 m/sec^2 for a distance of 18 m.

Typical charge-to-mass ratios of ice crystals generated by expelling liquid water through a nozzle into a vacuum measure 10^{-6} Coulomb/kg. The maximum possible charge that can exist on a particle can be computed by equating the self-energy of the charge distribution ($3/5\ Q^2/4\pi\epsilon_o r$) to the heat of vaporization of the material. For a 1-mm diameter sphere, this is 5×10^{-7} Coulombs or ~ 1 Coulomb/kg. Therefore, the field at the particle must be at least 8.7 volts/m to account for the motion. If this field results from the spacecraft potential, a potential of 1400 volts on the spacecraft would be required, assuming the spacecraft behaves as a uniformly charged sphere with a radius of 2 m. This is much greater than any potential expected on the spacecraft, which is typically a few volts [16]. Even in interplanetary space, the discharge current is on the order of 10^{-7} amps/m^2. This would discharge a 2-m sphere at the rate of 22 620 volts/sec; therefore, even if the spacecraft had achieved a high potential during the liquid dump, the potential could not remain for more than a few seconds. Furthermore, the particle appears to curve in a direction perpendicular to the line of sight. A charge interaction with the spacecraft would result in a curvature radius directed toward the spacecraft center. For these reasons, this observed curvature cannot be a result of an interaction with the spacecraft field..

This curvature cannot be caused by an interaction with a magnetic field either. For the maximum possible charge to mass of 1 Coulomb/kg moving at 2.5 m/sec, a magnetic field of 3.5 tesla (35 000 Gauss) would be required to produce the observed acceleration of 8.7 m/sec^2. Such a field is typical of what one would expect between the poles of a good magnet, not 18 m from a spacecraft.

Another possible cause for the observed motion would be an expulsion of material from the particle itself. Such material could be air trapped in the ice, or could be the ice sublimating. The average molecular air-molecules speed at ambient temperature is 476 m/sec. If these were jetted in a directed stream, 1.8 percent of the particle's mass would have to be lost per second to give the observed acceleration. The air density at cabin atmosphere (5 psi or 3.44×10^4 N/m^2) is 0.386 kg/m^3. The relative volume of voids to solid ice required for a 0.5-sec burst is 24/1. It seems unreasonable to expect the ice to have this much void volume and yet be somehow surrounded with an ice layer impervious to contain trapped gas.

If the ice particle is a total adsorber of solar radiation, the sublimation mass loss rate per unit mass is 0.07 percent per sec for a 1-mm-diameter particle. The bulk density would have to be less than 0.04 gm/cm^3 to increase this to the required value of 1.8 percent per sec. A further difficulty with this possibility is that the sun is below the lower left corner; whereas, the radius of curvature appears to be toward the lower right corner. Also, molecules sublimated from the surface would be ejected in essentially a cosine pattern about the subsolar point, thus further reducing the momentum imparted to the particle.

Perhaps a more reasonable possibility would be to consider particle-particle interactions. In fact, the hyperbolic shape of the trajectory suggests a repulsive electrostatic collision with a larger particle that is not in the field of view. From Coulomb's law, the product of charges required to produce an acceleration of 8.7 m/sec^2 at 2 m is

$$Q_1 Q_2 = -3.8 \times 10^{-9} \text{ m (Coulombs}^2\text{)}.$$

A 1-mm-diameter sphere of solid ice density has a mass of 5.2×10^{-7} kg; therefore, the product of the two charges is 2×10^{-15} Coulomb^2, which corresponds to 4.5×10^{-8} Coulombs each if the charge is equally divided. This is below the maximum possible charge; therefore, this mechanism is not impossible. Several other factors lend credence to this possibility. First, the assumed second particle could be much larger and, therefore, could carry a substantially larger portion of the required charge. Second, the observed particle could be, and probably is, much less dense than solid ice, thereby reducing the estimated mass and the required amount of charge. Finally, the fact that several particles appear to curve in the same general direction suggests a strong radial field originating somewhere below the lower right corner. The discharge current of 10^{-7} amps/m^2 mentioned earlier will discharge a 1-mm-diameter sphere at a rate of 5.6 volts/sec or 6.3×10^{-10} Coulombs/sec. Therefore, a high charge could exist for the few seconds required for the particle to arrive at the observation point.

CONCLUSIONS

It was demonstrated that photographs of stars as faint as 6.8 magnitude could be taken in daylight from an Apollo Command Module. The limiting factor for photographing faint stars was photon starvation rather than

background light. The background illumination was lower than $10^{-12.3}$ $B_{\odot}$ except in the vicinity of window smudges where the background is $10^{-11.71}$ $B_{\odot}$. These smudges are thought to be scattering of reflected moonlight or cabin light leaking through the dark hood. This is lower than the background predicted by earlier studies, and is approximately the level of the zodiacal light. Any difficulty in seeing stars in daylight from an Apollo spacecraft must be because of high ambient background from earth, moon, sun, or cabin lights. It cannot be attributed to a contamination cloud around the spacecraft.

Liquid dumps on Apollo produce a large cloud of particles, many large enough to appear as individual particles (millimeter to centimeter size range). Also produced is a vast cloud of smaller particles ranging from a few microns to submillimeter which scatter light but are not resolved as individual particles. The peak brightness of the dump cloud was estimated to be $\sim 10^{-9}$ $B_{\odot}$. The decay was predicted by computing the column density as a function of time after dump. A good fit was obtained to the observed decay until fresh material began leaving.

Some peculiarities are seen in the particle tracks. There is evidence that a few particles execute curved trajectories. Various mechanisms were investigated. The only plausible explanation appears to be a charged particle-charged particle interaction.

APPENDIX A. CALCULATIONS OF LIMITING MAGNITUDES

Using the fact that a $m_v = 0$ star outside the atmosphere produces an illuminance of 2.65×10^{-10} lumen/cm^2, and the definition of stellar magnitude, the illuminance of a m_v magnitude star is given by

$$I_o = 2.65 \times 10^{-6-.4m_v} \text{ lumen/m}^2 \quad . \tag{A-1}$$

The intensity on the film is given by equation (3),

$$I_{film} = I_o \frac{\pi \alpha^2 T}{4A_f} \tag{A-2}$$

where A_f is the area on the film plane subtended by the object. This area under ideal circumstances would be just the Airy disc of the lens. For diffraction-limited optics, the Airy disc has a diameter given by $1.22 \lambda f$ where λ is the wavelength and f is the f number. For the 18-mm lens used in this experiment, this would correspond to 0.55μ. However, the actual star images will be considerably larger than this because of the residual rates of the spacecraft, jitter of the spacecraft, and the fact that the actual Airy disc of the lens is larger than the diffraction-limited case. The actual measured images of g, h, h, and i Centarus in the 100-sec exposure are $20 \times 50\mu$. (See photomicrograph in Fig. 11.)

The threshold density required to be detectable above the 0.07 base fog is assumed to be 0.10. The exposures corresponding to the following tabulation are summarized in the table along with other pertinent data.

Exposure (sec)	Exposure Req. (m-candle-sec)	I_{film} (lumen/m^2)	Estimated Limiting Magnitude		
			Top	Middle	Bottom
1	0.029	0.0288	3.28	3.18	3.02
20	0.076	0.00388	5.45	5.35	5.21
60	0.100	0.00166	6.38	6.28	6.12
100	0.112	0.00112	6.80	6.70	6.53

APPENDIX B. INVESTIGATION OF STRAY LIGHT ON THE WINDOW

The scattered brightness of light from the spacecraft window can be computed from the relation

$$\frac{B}{B_O} = \frac{\omega_O}{\omega} \frac{I}{I_\Theta} \tag{B-1}$$

where ω is the field of the instrument. The scattered intensity for a scattering center on the window is

$$I = \frac{I_o}{r^2} \frac{d\sigma}{d\Omega} \tag{B-2}$$

where I_o is the illuminating intensity and $d\sigma/d\Omega$ is the differential cross section.

If a surface has N scattering centers in the field of view,

$$\frac{B}{B_O} = \frac{\omega_\Theta}{r^2\omega} \frac{I_o}{I_\Theta} N \frac{d\sigma}{d\Omega} \quad . \tag{B-3}$$

By definition of solid angle, $r^2\omega$ is the area of the window subtended by the detector. N $d\sigma/d\Omega$ is the total scattering cross section. Therefore, the ratio of the two is fraction of light scattered, S :

$$\frac{B}{B_\Theta} = \omega_\Theta \frac{I_o}{I_\Theta} S \quad . \tag{B-4}$$

Since the solid angle subtended by the sun is $\sim 6 \times 10^{-5}$ sr,

$$\frac{B}{B_{\odot}} = 6 \times 10^{-5} \frac{I_o}{I_O} S \quad . \tag{B-5}$$

The lunar phase angle was approximately 20 deg, for which the phase function is given by Allen [9] as 0 625. Since the spacecraft was approximately half the distance between the earth and moon, the luminous intensity will be increased by a factor of four. The ratio of I_{moon} to I_{sun} is, therefore,

$$\frac{I_{moon}}{I_{sun}} = 0.625 \times 4 \times 10^{.4(-26.78 + 12.70)} = 5.83 \times 10^{-6} \tag{B-6}$$

If moonlight was incident on the window, the brightness of scattered moonlight would be

$$B = 3.79 \times 10^{-10} S B_{\odot} \quad . \tag{B-7}$$

The observed value was $1.86 \times 10^{-12} B_O$.

Therefore, if moonlight were actually incident on the window, the observed brightness could be accounted for if the scatter fraction were 0.005. For normal incidence, Heinisch [17] found scattering values ranging from 0.0001 to 0.0005 for extremely clean single-pane windows, and values from 0.01 to 0.05 for "dirty" single-pane windows. A value 0.005 at grazing incidence for a triple window exposed for 272 hours in space plus pad and launch environment exposure does not seem unreasonable, but it is doubtful that direct moonlight was actually incident on the window since the nominal angle between the moon and the window is 108 deg.

Another source of light on the window is the moonlight scattered from the surfaces around the window opening. The intensity of moonlight scattered into an element of area dA_w on the window from an illuminated Lambertian surface dA_r is,

$$dI\, dA_w = I_r\, dA_r \cos\Theta \frac{d\Omega}{2\pi} \tag{B-8}$$

where I_r is the total scattered radiation $I_o(1 - \alpha)$ and $d\Omega$ is the solid angle subtended by dA_w

$$d\Omega = \frac{dA_w \cos i}{r^2} \tag{B-9}$$

where i is the angle of incidence of vector $\vec{r}$ from dA_r to dA_w. A curve integration over the illuminated surface estimated 6 percent of the reflected light incident near the top center of the window, 8 percent at the center, 11 percent at lower center, and 13 percent near the very bottom edge. Assuming that the absorption of the black paint used around the window opening is 0.9, the intensity ranges from 0.006 to 0.013 of the moon's intensity, or $3.5 \times 10^{-8}\ I_\odot$ to $7.6 \times 10^{-8}\ I_\odot$. From equation (B-5), the value of S would have to be 0.6 to produce the observed smudge near the center and 0.4 near the bottom. These appear unrealistically high.

A bright star on planet would have to have magnitude of -8.5 to equal the intensity of the reflected moonlight. This is far more intense than any combination of stars and planets.

Several possibilities exist. First, the reflected light from the antiglare shield may be considerably more than anticipated, particularly if the surface tends to backscatter. Second, there are shiny surfaces on the camera which could reflect the reflected moonlight back into the window, where it is multiplied, reflected, and scattered back into the lens. Third, there is a possibility that some light from the cabin leaked into the dark curtain and was incident on the window.

APPENDIX C. DIFFERENTIAL CROSS SECTION FOR A LAMBERTIAN SPHERE AT θ = 90 DEG

Consider a sphere with radius a . An element of surface area is $a^2 \sin\psi \, d\psi \, d\varphi$ where φ is the azimuth angle and ψ is the colatitude. Let the sphere be illuminated by parallel light in the direction $\varphi = 0$, $\psi = \pi/2$. The radiation incident on an element is $I_o \cos\varphi \sin\psi$, $-\pi/2 \leq \varphi \leq \pi/2$, $0 \leq \psi \leq \pi$. Let the viewing vector be in the direction $\varphi = \pi/2$, $\psi = \pi/2$. If the surface is perfectly diffuse (Lambertian surface), the scattered radiation is proportional to the incident radiation times the cosine of the angle between the element and the viewing vector, given by $\sin\varphi \sin\psi$. The observed intensity is, therefore,

$$I_{obs} = \int_0^{\pi/2} d\varphi \int_0^{\pi} d\psi \, I_o \cos\varphi \sin\varphi \sin^3\psi \, \frac{a^2}{r^2} \qquad \text{(C-1)}$$

$$I_{obs} = \frac{2}{3} \frac{a^2}{r^2} I_o \quad . \qquad \text{(C-2)}$$

From equation (7), the cross section is

$$\frac{d\sigma}{D\Omega} = \frac{2}{3} a^2 \quad . \qquad \text{(C-3)}$$

APPENDIX D. SPREAD OF DEFOCUSED IMAGE

An object located at o will form an image at i where o and i are related by

$$1/o + 1/i = 1/F \qquad \text{(D-1)}$$

If the lens is focused at infinity, the film will be located at the focal length F . The difference δ between i and F is

$$\delta = i - F = \frac{oF}{o - F} - F = \frac{F^2}{o - F} \quad . \qquad \text{(D-2)}$$

The rays coming through the outer edge of the aperture having diameter d will form a circle with diameter d_f on the film, which by similar triangles is given by

$$\frac{d_f}{\delta} = \frac{d}{i} = \frac{d}{oF}(o - F) \qquad \text{(D-3)}$$

From equation (D-2),

$$d_f = \frac{Fd}{o} \quad .$$

For F = 18 mm, and d = 20 mm, if d_f is to be less than 20 microns, o must be

$$o = \frac{18 \times 10^{-3}\ 20 \times 10^{-3}}{20 \times 10^{-6}} = 18 \text{ m} \quad .$$

REFERENCES

1. Newkirk, G. N.: The Optical Environment of Manned Spacecraft. Planet. Space Sci. 15, 1967, pp. 1267-1285.

2. Kovar, N. S., Kovar, R. P., and Bonner, G. P.: Light Scattering by Manned Spacecraft Atmospheres. Planet. Space Sci. 17, 1969, pp. 143-154.

3. Grobman, W. D., and Buffalano, C.: New Conclusions Concerning the Observation of Faint Sources from a Sunlit Spacecraft. Planet. Space Sci. 17, 1969, pp. 1089-1096.

4. Buffalano, A. C., Kratage, M. L., and Sharma, R. D.: Interpretation of Visual Observations of Apollo Water Dumps - Case 340. Bellcomm Memorandum B71 07014, July 14, 1971.

5. Star Atlas of Reference Stars and Nonstellar Objects. Smithsonian Astrophysical Observatory, 1967.

6. Star Catalog. Smithsonian Astrophysical Observatory, 1966.

7. Norton, A. P., and Inglis, J. G.: Norton's Star Atlas and Reference Handbook. Sky Publishing Corporation, Cambridge, 1964.

8. Gooding, R. A.: Reciprocity Behavior on SO-164 Film. Technicolor, Inc., Task Order HT-31, September 29, 1971.

9. Allen, C. W.: Astrophysical Quantities. University of London, 1963.

10. Analysis of Apollo 8 Photography and Visual Observations. NASA SP-201, 1969.

11. Kerker, M.: The Scattering of Light. Academic Press, N. Y., 1969, p. 84.

12. Van De Hulst, H. C.: Light Scattering by Small Particles. Wiley, New York, 1962, p. 108.

13. Irving, J., and Mullineux, N.: Mathematics in Physics and Engineering. Academic Press, New York, 1959, p. 131.

REFERENCES (Concluded)

14. Mie, G.: Beitrage Zur Optik Arriber Medien. Ann. Physik, 25, 1908, pp. 377-445.

15. Bicket, N. A., and Gary, G. A.: Mie Scattering: A Computer Program and an Atlas. NASA TMX 53951, September 29, 1969.

16. West, W. S., Gore, J. V., Kasha, M. A., and Bilsky, H. W.: Spacecraft Charge Buildup Analysis. NASA SP-276, 1971.

17. Heinisch, R. P.: Study of Visual Detection of Stars in a Spacecraft Environment. Honeywell Doc. 12127, NASA Contract NAS2-5015, April 1969.

APPROVAL

APOLLO 15 CONTAMINATION PHOTOGRAPHY

By R. J. Naumann

The information in this report has been reviewed for security classification. Review of any information concerning Department of Defense or Atomic Energy Commission programs has been made by the MSFC Security Classification Officer. This report, in its entirety, has been determined to be unclassified

This document has also been reviewed and approved for technical accuracy

Gerhard B Heller

GERHARD B. HELLER
Director, Space Sciences Laboratory

☆ U S GOVERNMENT PRINTING OFFICE 1972 — 746 821/4715 REGION NO 4

DISTRIBUTION

INTERNAL

DEP-T
W Lucas

AD-S
E Stuhlinger

PM-SAT-MGR
R G Smith

PM-SL-El
R Pace

PM-SL-DP
J Waite

S&E-R-DIR
W G Johnson

S&E-ASTN-ME
R Gause

S&E-ASTN-MEV
J Horton

S&E-ASTN-PL
J Moses

S&E-CSE-A
R Edwards

S&E-CSE-AS
C Davis

S&E-QUAL-AE
M Pickard

S&E-SSL-DIR
G Heller

S&E-SSL-X
J Dozier
H Weathers (5)

S&E-SSL-N
R Decher

S&E-SSL-P
R Naumann (15)

S&E-SSL-S
W Sieber

S&E-SSL-T
W Snoddy

S&E-SSL-TT
A Gary
P Craven

S&E-SSL-C
Reserve (10)

A&TS-PAT
L D Wofford, Jr

A&TS-MS-H

A&TS-MS-IP (2)

A&TS-MS-IL (8)

A&TS-TU (6)

EXTERNAL

Scientific and Technical Information Facility (25)
P O Box 33
College Park, Maryland 20740
Attn NASA Representative (S-AK/RKT)

National Aeronautics and Space Administration
Washington, D C 20546
G Vacca, MLE
L Werner, MLA
G Deutsch, RW
I Weinburg, RWM
D Novik, RS
M Dubin, SGM
A Reetz, RX

Lewis Research Center
21000 Brookpark Road
Cleveland, Ohio 44135
Attn Dr H Mark, M S 301

John F Kennedy Space Center
Kennedy Space Center, Florida 32899
Attn R. Bland, AA-SVO-3

Manned Spacecraft Center
Houston, Texas 77058
Dr C Henize, CB
Col D Scott, CB
Lt Col A Worden, CB
Dr P Chapman, CB
Col K Mattingly, CB
G Cress, FC8
G Bonner, TG4
C Charlesworth, KA
C Glancy, PD4 (5)
A Larsen, FCA
R Kubicki, PA
K Kleinknecht, KA
N Hardee, TD-43

Goddard Space Flight Center
Greenbelt, Maryland 20771
A. Lekebusch, Code 320
Dr C Buffalano, Code 110

Langley Research Center
Hampton, Virginia 23365
Attn W. Lassiter, M S 187

Martin Marietta Corporation
P O Box 179
Denver, Colorado 80201
Attn Dr Joe Muscari
Dr E Ress
Dr R Ellison

Naval Research Laboratory
Washington, D C 20390
Attn Dr R Tousey
Mr Bill Hunter, Code 7143

High Altitude Observatory
National Center for Atmospheric Research
P. O Box 1550
Boulder, Colorado 80302
Attn Dr R McQueen

Dudley Observatory
100 Fuller Road
Albany, New York 12205
Attn Dr J L Weinberg
Dr Curtis L Hemenway

Laboratoire d'Astronomie Spatiale
Centre National de La Recherche Scientifique
Marseilles, France
Attn Dr Georges Courtes

General Electric Company
Space Sciences Laboratory
Valley Forge Space Technology Center
P O Box 8555
Philadelphia, Pennsylvania 19101
Attn Dr H W Goldstein

General Dynamics Corp
Convair Division
P O Box 1128
San Diego, California 92112
Attn Dr T Neu

Particle Measuring Systems
Clarendon Hills, Illinois 60514
Attn Dr Robert G Knollenberg

MTS, Materials Sciences Laboratory
Aerospace Corporation
P O Box 95085
Los Angeles, California 90045
Attn Dr E N Borson

Dr. Ravi D Sharma
955 L'Enfant Plaza North, S W
Washington, D C 20024

Faraday Laboratories, Inc
7742 Herschel Avenue
La Jolla, California 92037
Attn Dr Dan McKeown

TRW, Inc
1 Space Park Drive
Houston, Texas 77058
Attn Jim Scott

University of Texas, Dallas
Dallas, Texas 35201
Attn Dr John Hoffman

Johns Hopkins University
Baltimore, Maryland 21218
Attn Dr William Fastie

Lockheed Electronics Co
16811 El Camino Real
Houston, Texas 75058
Attn Mr Wesley Simpson, CO3

Technicolor, Inc
1730 NASA Boulevard
Houston, Texas 77058
Attn Bob Gooding